# Validation of ICESat-2 ATL08 Terrain and Canopy Height Retrievals in Tropical Mesoamerican Forests

Juan Carlos Fernandez-Diaz, *Member, IEEE*, Mariya Velikova, and Craig L. Glennie, *Member, IEEE*

***Abstract*—In this article, we validate Ice, Cloud, and Land Elevation Satellite2 (ICESat-2)-derived interpolated terrain elevations (h_te_interp), top of canopy elevations (h_canopy_abs), and estimated canopy heights (h_canopy) in dense tropical forests of Mexico, Belize, Guatemala, and Honduras. Data from close to 30 000 ICESat-2 ATL-08 segments are compared against parameters derived from high-density (>15 pulses/m$^2$) topographic airborne lidar (HDL) data from seven different sites with a variety of forest structure and terrain conditions, totaling 3742 km$^2$ of validated area. Our results indicate that in these high closure forests the range of errors (within the 5th to 95th percentiles) for these parameters vary widely, but their median and interquartile range (IQR) grow proportionally to the HDL-derived reference canopy height (rCH). The errors in h_te_interp retrieval grow in proportion to the rCH from ±2.5 m for areas with fairly low rCH (5–10 m) all the way to −10 to 24 m for areas with rCH of 40–45 m. The median of h_te_interp errors also grows proportionally to rCH and is consistently overestimated with regards to the reference. With respect to h_canopy_abs, it was observed that the errors also grow with increasing rCH but a much lower rate; the IQR is generally constrained between −5.5 and 6.0 m, while the median remains mostly uniform and independent of the rCH and underestimates the reference by −0.5–−2.0 m. The IQR of the errors in h_canopy normalized to rCH exhibits a mostly uniform behavior across the range of rCH between −33.5% and 7.0%, with the median fluctuating around an underestimation level of –16.5%.**

***Index Terms*—Laser radar, lidar, remote sensing, terrain mapping, vegetation mapping.**

## I. Introduction

TOPOGRAPHY and vegetation mapping in three-dimensions (3-D) are fundamental problems in the geosciences [1]. NASA's Ice, Cloud, and Land Elevation Satellites (ICESat and ICESat-2) have the primary mission of mapping the topography of the cryosphere at a global scale, and as secondary mission objectives, mapping of vegetation heights [2], [3]. Forests play a significant role in terrestrial carbon sequestration by storage in soil organic matter and their living biomass (vegetation). Tropical forests account for a quarter to two-thirds of all terrestrial biomass [4], [5] and it is estimated that at least two-thirds of the planet's biodiversity inhabit tropical forests [6]; unfortunately, the tropics are the most threatened forests in the world [5].

Because of their extent, dense canopy and obscuring atmospheric phenomena (clouds) in tropical regions, studying these forests is extremely challenging. Airborne mapping lidar or airborne laser scanning (ALS) has become one of the most accurate and fine-resolution technological choices for 3-D mapping of terrain and forest structure at coverages that range from tens to hundreds of thousands of km$^2$ [7]. Some limitations of ALS include high cost, limited coverage footprint, and lack of repeat observations. Spaceborne lidar sensors have the potential to overcome some of these limitations, however, they face unique challenges related to their limited optical power that needs to be distributed either to finely record the vertical structure of forests at limited horizontal sampling or at an increased horizontal sampling with decreased vertical structure resolution. The Geoscience Laser Altimeter System (GLAS) instrument onboard the ICESat mission [2] and the Global Ecosystem Dynamics Investigation Lidar (GEDI) sensor [8] attached to the International Space Station focus on vertical structure (linear mode full waveform), while the Advanced Topographic Laser Altimeter System (ATLAS) instrument onboard ICESat-2 operates with increased horizontal resolution using single photon detection [3].

While the ATLAS sensor design is optimized for the ICESat-2 primary mission to accurately map the topography of the cryosphere, it may also be successful in accurately mapping canopy heights in most forest environments. However, tropical forests, because of their canopy structure (height, density, and closure) and the occurrence of atmospheric obscuring phenomena present the most challenging conditions for canopy height retrieval. Because the ATLAS-derived canopy heights can be important input for the estimation of above-ground biomass and a critical component in carbon balance studies [9], the validation of data obtained from such novel sensors under diverse geographical and forest conditions is an important ongoing research activity.

Validation, in its most basic form, consists of comparison of remotely sensed geophysical observations or biophysical parameters to values derived from methods considered to have greater accuracy and precision. As depicted in Fig. 1, this article, similar to other articles, aims to validate ATLAS-derived terrain geodetic elevations and canopy heights against similar values derived from ALS. Validation of terrain elevations derived from ATLAS observations have been reported in [10]–[12]; assessments of

Manuscript received November 3, 2021; revised January 27, 2022 and March 11, 2022; accepted March 15, 2022. Date of publication March 29, 2022; date of current version April 26, 2022. This work was supported by the United States National Science Foundation Division of Earth Sciences, Instrumentation, and Facilities Program under Grant 1830734. *(Corresponding author: Juan Carlos Fernandez-Diaz.)*

The authors are with the National Center for Airborne Laser Mapping, University of Houston, Houston, TX 77204 USA (e-mail: jfernan4@central.uh.edu; mgveliko@cougarnet.uh.edu; clglennie@uh.edu).

Digital Object Identifier 10.1109/JSTARS.2022.3163208

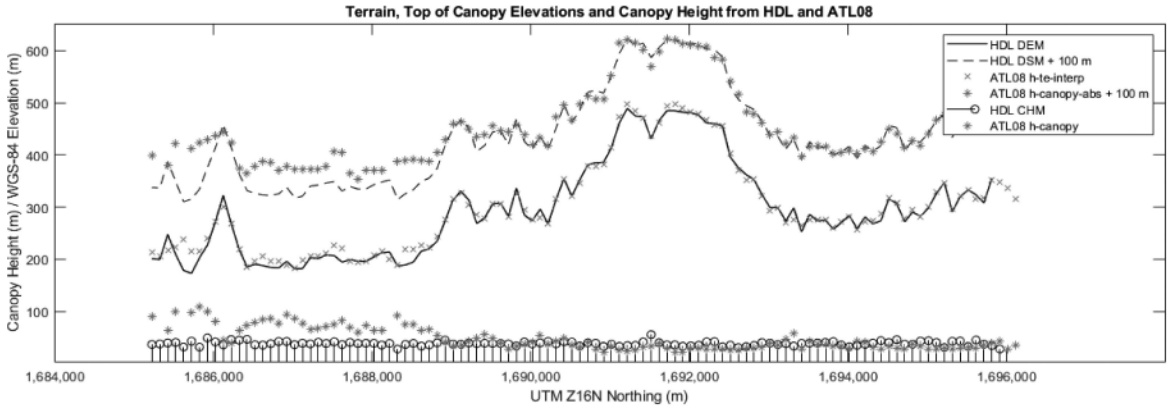


Fig. 1. Example profile comparing HDL and ATL08 terrain and top of canopy geodetic elevations above the WGS-84 ellipsoid as well as relative canopy heights. Top of canopy elevations were offset by +100 m for clarity. Left third of the figure shows significant top of canopy retrieval errors despite relatively good terrain retrieval, resulting in significant canopy height errors.

both terrain elevation and canopy heights have been reported in [13]–[16]; and of canopy heights exclusively in [17]. While the above articles are conducted mostly in boreal, temperate, and subtropical forests with a very few samples in tropical savannas and forests, the results presented in this communication are, to our knowledge, the first validation conducted over large areas in a varied sample of tropical forests in the western hemisphere using high-density (>15 pulses/m$^2$), linear-mode, discrete, and topographic airborne lidar data (HDL-high-density lidar) as a reference. Because of the unique structural characteristics (openness, density, and height) of the tropical forest used in our validation, our results are both unique and complementary to those previously reported. For instance, Malambo and Popescu [16] concluded that the best performance for canopy heights was observed when canopy cover was greater than 80%, and that ATL08 observations for canopy heights are more suitable in relatively dense canopy environments (conifer and broadleaf) over environments with sparse vegetation (grassland and savannas). Our validation in tropical forests indicates that their conclusion is partially true; relatively good agreement is observed in the retrieval of top of canopy elevations when the canopy closure and height are very high; however, the ATLAS observations and algorithms have considerable difficulty retrieving the underlying terrain elevations, consistent with what is reported in [14]. This in turn reduces the accuracy of the relative canopy heights which are derived by subtracting the terrain elevation from the top of canopy elevations. Another distinguishing factor of our article is that the HDL used as a reference have canopy measurements in excess of 20 returns (points)/m$^2$, which allow for accurate mapping of the top of these dense forests, enabling the validation of both the ATLAS-derived top of canopy elevation (h_canopy_abs) and canopy heights (h_canopy) independently, while other articles focus mostly on h_canopy and height percentiles.

As noted in other articles [14]–[16], there are limitations and challenges to the validation of spaceborne observations using field data. These challenges are important to address, so we briefly list them in order of significance below, and then expand on them where appropriate in subsequent sections. The most significant challenges are 1) temporal differences between the ATLAS and HDL observations, 2) different footprint diameter and the geolocation uncertainty for ATLAS, 3) limited geographic coverage compared to the ICESat-2 global scope, and 4) top of canopy is based on the 98th percentile elevation of the ATLAS photo events versus elevation of highest return for HDL observations. Other differences that have been assessed to be miniscule (cm level) compared to the magnitude of the retrieval errors (decimeter to meters) include offsets between ATL08 and HDL WGS-84 realizations and reference benchmarks; however, these do not affect the canopy height values as it is a relative measurement.

Given that the above limitations have been mitigated as best as possible, and because the results presented within are different and complementary to what has been reported before, this article represents a significant contribution toward the understanding of the potential and limitations of ICESat-2 retrieval of terrain and forest structure in Mesoamerican tropical forests specifically, but also could be cautiously extrapolated to tropical environments elsewhere. The article presented here characterizes the errors in the ATLAS-derived interpolated terrain elevation (h_te_interp), top of canopy elevation (h_canopy_abs), and estimated canopy height (h_canopy) as they relate to the HDL reference canopy height (rCH) and further presents trends for in the median of these errors based on day/night observation time and weak/strong ATLAS beams. Due to both the ongoing ICESat-2 data validation efforts, the use of the validated ATL08 transect product serving as input for a 500-m rasterized canopy height product (ATL18) [3], and because ATLAS data will be used as inputs in many kinds of biophysical investigations, we consider that a brief and timely publication of selected results for tropical regions is of importance to the research community.

## II. Materials and Methods

### A. *ICESat-2 ATL08 Data*

The ICESat-2 data product relevant to this article is the ATLAS/ICESat-2 L3A land and vegetation height product designated ATL08, which presents along-track terrain and top of canopy elevations above the WGS84 ellipsoid (ITRF2014 reference frame) as well as vegetation canopy height in fixed 100-m

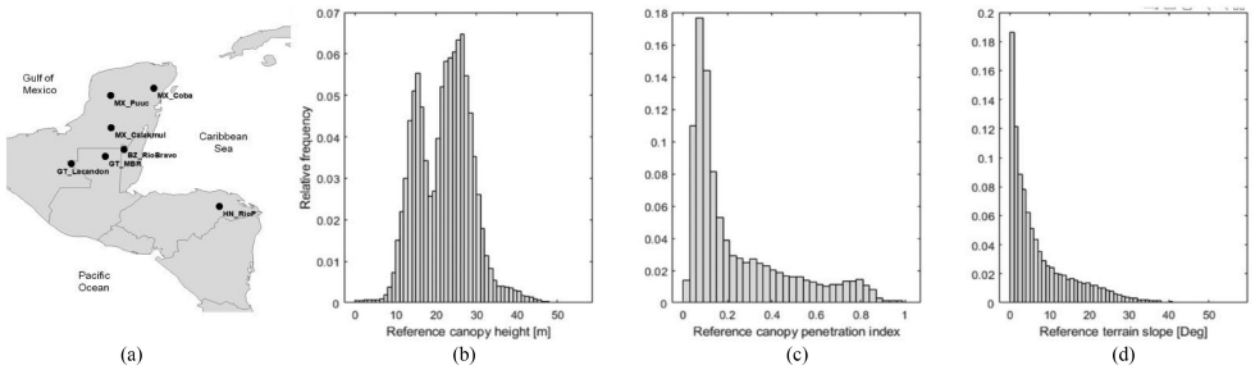


Fig. 2. Metadata for the reference HDL data used for validation. (a) Location of distributed test areas. (b) Canopy height (CH). (c) Canopy penetration index. (d) Terrain slope.

TABLE I
DETAILS OF VALIDATED ATL08 SAMPLES PER TEST AREA

| Validation Area | Δt years | OP/BT | # Seg / % Tot |
|---|---|---|---|
| Maya BR, Guatemala [24] | -0.68 / 1.31 | 11 / 59 | 20,353/69.0% |
| Puuc, Mexico [26] | 1.55 / 3.29 | 5 / 20 | 1431 / 4.9% |
| Lacandon, Guatemala [29] | -0.37 / 1.38 | 8 / 19 | 895 / 3.0% |
| Coba, Mexico [25] | 1.72 / 3.46 | 5 / 9 | 543 / 1.8% |
| Calakmul BR, Mexico [28] | 2.44 / 4.43 | 7 / 31 | 3816 / 12.9% |
| Rio Bravo R, Belize [27] | 2.47 / 4.29 | 11 / 33 | 1842 / 6.3% |
| Rio Platano R, Honduras [23] | 6.49 / 8.31 | 4 / 16 | 604 / 2.1% |

$\Delta t$: min and max of time between reference and ATLAS acquisitions (ATL08-HDL), OP: # of orbital passes, BT: # of beam tracks, Seg: # of ATL08 h_te_interp samples validated, and %Tot: percentage for area of total segments (29 484). BR is abbreviation for biosphere reserve and R for reserve.

along-track profile segments, with an internal breakdown of 20-m subsegments in the data structure (Fig. 1). The ATL08 product contains over 30 variables related to the estimated elevations and heights with internally computed uncertainties [3], [18]. For this article, we extracted data for nine variables within the ATL08 hierarchical data format (HDF5) file including their reported internal uncertainties. Besides the segment center geographic position (latitude and longitude), the most relevant for the study are h_te_interp (interpolated terrain surface height at mid-point of segment), h_te_mean (mean of the terrain heights), h_canopy_abs (98% height of individual canopy elevations above the ellipsoid), and h_canopy (the 98% height of individual relative canopy heights). For more information on these and all the variables in the ATL08 product, the reader is referred to [18].

We used ATLAS data collected between October 24, 2018 and October, 28 2020, corresponding to orbital cycles 1–9 which included 20 different ground reference tracks, all generated by processing version 3 [18]. This date range was selected to minimize the temporal difference between ATLAS and HDL data (Table I). Furthermore, to minimize temporal differences, the validation samples were selected from late succession forests which exhibit less growth than younger forests. The temporal differences mostly affect the validation of canopy parameters, and changes in terrain elevation are negligible. The minimum temporal difference for data used in this article is a couple of weeks, and for 97.9% of the validation samples it is less than 4.5 years; the maximum being 8.3 years (Table I). ATLAS ATL08 HDF files were downloaded from the National Snow and Ice Data Center after data availability and quality was assessed though OpenAltimetry [19].

### B. *Linear-Mode Airborne High Density Lidar (HDL)*

HDL data with densities greater than 15 pulses/m$^2$ were used as reference for the validation of the ATL08 products; because up to four returns can be recorded per pulse by the airborne instruments used, canopy measurement densities are in excess of 20 returns (points)/m$^2$. The selection of the validations sites considered 1) minimizing the temporal difference between ATLAS and HDL collections, 2) selecting sites in protected or reserve areas with old growth forests and minimal to no anthropogenic change, and 3) sites with diverse forest structure and topographic characteristics. Based on these criteria, seven sites were selected (Fig. 2), three on the Yucatan peninsula of Mexico, two in Guatemala, one in Belize, and one in the Mosquitia region of Honduras. These HDL reference datasets were collected by the National Center for Airborne Laser Mapping (NCALM) with the specific goal of optimizing canopy penetration to obtain high fidelity and accuracy digital elevation models (DEM) [20]. A total of 97.9% of the HDL validation measurements came from data collected with the Teledyne Optech Titan multispectral lidar [21]. While there are slight differences in the collection parameters of the reference HDL datasets due to changes in project specific target pulse densities and flight conditions, in general, they were collected from heights above ground lower than 700 m and with scan angles between $\pm$ 25° to 30°; all flight lines have 50% lateral overlap with adjacent swaths. In addition, every flight line is collected from three different look angles (nadir, 3.5° and 7.0° forward of nadir), so at a minimum every square meter of the target surface is scanned from six different geometries (three forward look angles $\times$ two relative positions within the swath) [21].

While a full evaluation of the absolute positional accuracy of HDL terrain elevations under forest canopies has not been conducted because of the impracticality to conduct such tests over large areas, it is estimated at better than 15 cm vertically based on precision assessments in nearby open and flat areas

[with precision normally better than 8 cm root mean square error (RMSE)] based on procedures reported in [21] and [22]. Furthermore, all of the resultant DEMs have been extensively analyzed and field-verified for archaeological prospection, revealing a high level of fidelity and internal accuracy as reported in publications including, but not limited to [23]–[29].

The Honduras Mosquitia HDL validation dataset represents only 2.1% of our samples, and has different characteristics than the other HDL sets. It is the only one collected with an Optech Gemini sensor, which is a generation older than the Teledyne Optech Titan lidar [21], and it is also the reference dataset with the largest temporal difference between HDL and ATLAS collections of 6.5–8.3 years (Table I). However, we consider it to be extremely important as it presents forest samples with the highest canopy closure, density, and heights accessible to us; in addition, it contains steeper slopes than any other validation area (Fig. 1). Thus, it represents one of the most challenging environments for accurate ATLAS terrain and canopy retrieval.

It is important to note that the methods for computation of top of canopy and the resultant canopy heights from the reference HDL data differ from the methods used on the ATLAS observations and reported in the ATL08 files. Given the photon-counting design of the ATLAS sensor, with extremely high sensitivity and thus subject to significant noise, the top of canopy elevation (h_canopy_abs) and its relative height above the ground (h_canopy) are given by the elevation of the 98th percentile photon-event. This is in order to reduce the possibility that a noise photon-event could be incorrectly labeled as a canopy photon [14], [18]. Other articles such as [14] and [16], which have used ALS data as reference for their validation, compare the ATL08 98th percentile elevation to the equivalent 98th percentile of the ALS return elevations. While we agree that there is a good technical reason to limit the top of canopy of ATLAS observations to the 98-percentile elevation of photon-events, we do not believe there is a technical reason to apply the same definition to the top of canopy for linear mode and discrete return ALS data. On the contrary, data for our particular study areas indicate that considering the 98th percentile instead of the maximum elevation of the HDL data could lead to underestimation of the rCH by up to several meters; this could potentially produce lower validation error metrics, but will significantly bias the assessment. Thus, in this article, we used the geodetic elevation of the highest return within the analysis unit (20 m $\times$ 20 m cell) as the reference top of canopy elevation. We believe that given the extreme care taken during the collection and processing of the reference HDL data (expanded below), and that this constitutes the most accurate definition of top of canopy elevation and the associated canopy height. This interpretation of canopy height is also sustained by the findings of a recent study that tested different methods and metrics aimed at obtaining the highest accuracy for this parameter [30].

We are confident that the highest HDL elevation within a study cell is the most accurate definition for top of canopy elevation because extreme care has been taken in the collection and processing of the HDL observations. The HDL data were collected with the goal of maximizing canopy penetration; because of this the high pulse density coupled with the sensor beam divergence has the effect of illuminating the entire target surface multiple times and from different look angles [21]. These factors represent a substantial difference to other assessments that used lower density ALS data as a validation reference and which likely had difficulty sampling or detecting the highest elevation in the canopy—leading to an underestimation of canopy height. Neuenschwander *et al.* [14] report a minimum measurement density of 0.5 pts/m$^2$ for their study area in Finland; Liu *et al.* [15] used NEON data for 40 sites distributed across the USA including sites in Hawaii and Alaska with 1 to 4 pts/m$^2$; Malambo and Popescu [16] reported data for 12 sites across the contiguous USA, with varying densities that for the most part range between 3 and 11 pts/m$^2$. In addition, during the processing of our HDL data, isolated return algorithms which aim at identifying spurious returns (returns with no neighboring points within a 3-m diameter sphere) were run to flag these as potential noise not considered for terrain or canopy computations.

Finally, the collection and processing of the HDL datasets have been conducted by a single provider with predominantly the same equipment and processing procedures. The datasets have also been extensively validated. Therefore, these reference datasets likely have higher consistency and accuracy when compared to reference HDL observations for the majority of other assessments conducted with data generated from disparate sensors, collection, and processing procedures.

### C. Validation Procedure

Although the validation presented here is based on the availability of reference data, we approach the analysis as an end user of the ATL08 products without access to external data that would allow the removal of outliers or the minimization of ATL08 geolocation errors. Our objective is to characterize the absolute errors present in our sample of ATL08 data as produced and published; in agreement with the procedures recommended by the American Society for Photogrammetry and Remote Sensing (ASPRS) in their Positional Accuracy Standards for Digital Geospatial Data [22]. This ASPRS standard establishes that "vertical accuracy shall be tested by comparing the elevations of the surface represented by the data set with elevations determined from an independent source of higher accuracy. This is done by comparing the elevations of the checkpoints with elevations interpolated from the data set at the same *x*/*y* coordinates." The standard does not allow for horizontal shifting or other kind of manipulation of the test dataset to obtain a higher accuracy value.

Our procedure is in contrast to the methodology followed in [14] and [16], where the ATLAS data is dynamically displaced both along and across track to minimize elevation differences. We recognize that geolocation correction is in itself a form of horizontal accuracy assessment and an important exercise. As such we have tested adjustments on roughly a quarter of our ATL08 validation segments using shifts calculated with the software package PhoREAL developed for processing of ATL03 and ATL08 data by the Applied Research Laboratories of the University of Texas at Austin[1]; and which has been used in other published validations. However, because of the tall

[1][Online]. Available: https://github.com/icesat-2UT/PhoREAL

and closed forest canopies tested, the reported ATL08 terrain elevations (h_te_interp and h_te_mean) are noisy and usually overestimated and as a result the PhoREAL algorithm for terrain surface matching between the ATLAS (ATL03 and ATL08) and reference data does not produce consistent or reliable displacement values. We deem them inconsistent because they usually provide contradictory offset directions when individually determined for the different beams, and unreliable because in many cases the offsets are much larger than the expected horizontal and vertical uncertainties for ATLAS data. Our generalized observations regarding the over-corrections suggested by PhoREAL are consistent with what was reported by [16] for the subtropical test sites in Louisiana where the automated shifts were considered "unreliable" and had to be determined "manually."

Further, our results comparing aggregated retrieval error metrics on ATL08 data before and after geolocation adjustment indicate that while minuscule improvements in h_te_interp retrieval are obtained for certain ATLAS profiles it is not the case in the aggregate. At the same time, h_canopy_abs retrieval accuracy is degraded with no significant change in the retrieval accuracy of h_canopy due to the high spatial autocorrelation of this biophysical parameter (see Appendix and Table VII for the overall geolocation adjustment results and Table VIII for the per beam/pass results). Extensive development and testing of procedures for geolocation adjustment for research applications of ATLAS data in areas with dense vegetation needs further research and it is outside the scope of this assessment.

It is important to note that for our validation we considered all available ATL08 100-m segment data with spatially coincident HDL reference data, without any removal of outliers. While this produces higher error metric values for the assessed parameters, it better characterizes the full range of errors present in the ATL08 data that would be observed from the perspective of an end user.

Given that the ATLAS (test) and HDL (reference) datasets were collected and processed in significantly different fashions: the ATLAS observations were recorded in individual transects from laser footprints specified to have a diameter of less than 17.5 m [3] and with photon-events referenced to geocentric (latitude and longitude) coordinates; while the HDL is merged swaths with individual footprints of 0.3 to 1 m recorded in projected (UTM) coordinates. Therefore, significant effort went into reprocessing and transforming both datasets to ensure consistent, repeatable, and valid comparisons.

The entire validation process was conducted through Matlab scripts. In the first step, the script reads the HDF5 files and for each ATL08 segment available within the HDL data boundaries, the segment center latitude and longitude are converted to UTM northing and easting coordinates in the zone matching the HDL. For each segment center point, four additional UTM coordinates were generated between ATL08 samples at 20-m spacing ($-40$, $-20$, 20, and 40 m), see Fig. 3. These additional points should closely match the center locations of the 20-m subsegments in the ATL08 structure. For each of these points (including the center), values of the parameters of interest were extracted from the HDL reference rasters.

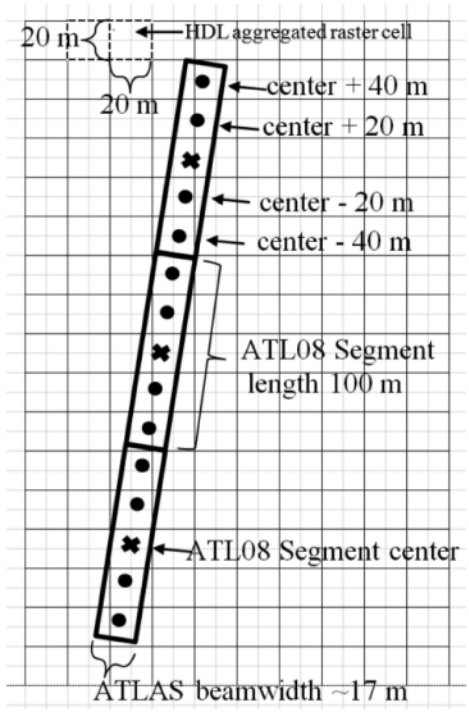


Fig. 3. Diagram illustrating the HDL sampling strategy to match the ATL08 segment geometry.

The HDL data in the form of point clouds (PC) and rasters was carefully processed and thoroughly inspected and field validated for archaeological prospection projects. Because the project areas are in forested areas, with little-to-no modern development (building, roads, etc.), the PC stored in LAS format has been classified into basic classes: ground, vegetation, and outliers (usually multipath and atmospheric returns—typically $<0.1\%$ of observations). Each return in the PC contains elevation above the WGS-84 ellipsoid as well as many other attributes such as class, pulse time, flight line, scan angle, intensity, and return order [31], [32]. The original rasters intended for archaeological prospection are terrain DEM and first surface elevation models (DSM) created with spacing of 0.5–1 m through Kriging interpolation from the classified PC as per NCALM procedures described in [33].

The original DEMs and DSMs were smoothed using a uniform kernel and then subsampled into 20-m rasters. This spacing was selected for two main reasons: to match the 20-m subsegment unit of the ATL08 and to match the ATLAS footprint and allow for a portion of ATLAS positional uncertainty (Fig. 3). By design specifications, the ATLAS footprint should be less than 17.5 m in diameter and the positional uncertainty lower than 6.5 m [3]. On-orbit assesments in Antarctica and New Mexico, USA (sites with low atmospheric humidity) have provided measurements of footprint diameters in the range of 8.3–12.4 m ($10.9 \pm 1.2$ m) and radial positional uncertainties in the range of 0.4 to 8.5 m ($3.5 \pm 2.1$ m) [34], [35].

The subsampled rasters represent 1) terrain and 2) top of canopy elevations with respect to the WGS-84 ellipsoid. Additional HDL reference rasters include 3) terrain slope gradient, 4) rCH, and 5) laser penetration index as a proxy for canopy

openness or closure (Fig. 2). The terrain slope gradient was computed using Golden Software Surfer which reports the cell-to-cell slope for the direction of highest change. The canopy height (rCH) rasters were created from the PC in TerraSolid Terrascan by computing the distance for each return to a triangulated ground surface model (based on classified ground returns) and identifying the return with the maximum height above ground within the $20 \times 20$ raster cell. The laser penetration index raster was created in Surfer by computing the fraction of laser pulses that produced ground returns through the division of ground density by raw pulse density rasters.

For each center point of the ATL08 segment and the four additional points ($-40$, $-20$, 20, and 40 m) in UTM coordinates, reference values were extracted from the HDL rasters through bilinear interpolation considering the four nearest raster cells (Fig. 3). The reference values for each of these five samples were then aggregated into a single value using descriptive statistics which best match the ATL08 parameters under assessment. For instance, the ATL08 h_te_interp value was compared to the HDL terrain elevation value extracted for the central point only, while ATL08 mean terrain segment elevation (h_te_mean) was compared to the average of the five extracted elevations. The ATL08 h_canopy was compared to the maximum of the five HDL CH extracted for each of the validation points.

The per sample (matching ATL08 segment and aggregated HDL metric) retrieval errors were computed by subtracting the HDL reference values from the ATL08 values

$$\text{error}_{\text{sample } i} = h_{\text{ATL08 } i} - h_{\text{HDL } i} \tag{1}$$

For the canopy height a per sample normalized error was computed as

$$n\_\text{error}_{\text{sample } i} = \frac{\text{ch}_{\text{ATL08 } i} - \text{ch}_{\text{HDL } i}}{\text{ch}_{\text{HDL i}}} = \frac{\text{eCH} - \text{rCH}}{\text{rCH}} \tag{2}$$

From sample errors, aggregated error metrics such as RMSE, mean absolute error (MAE), and coefficient of determination ($R^2$) were computed as

$$\text{RMSE} = \sqrt{\frac{1}{n}\sum_{i=1}^{n}\left(\text{error}_{\text{sample } i}\right)^2} \tag{3}$$

$$\text{MAE} = \frac{1}{n}\sum_{i=1}^{n}\left|\text{error}_{\text{sample } i}\right| \tag{4}$$

$$R^2 = 1 - \frac{\sum_{i=1}^{n}\left(\text{error}_{\text{sample } i}\right)^2}{\sum_{i=1}^{n}\left(h_{\text{HDL } i} - \text{mean}\left(h_{\text{HDL all}}\right)\right)^2}. \tag{5}$$

In addition, descriptive statistics (min, mean, median, maximum, standard deviation, and 5th and 95th percentiles) of the errors were computed for the entire set (overall) and selected groups of observations (per beam/pass, per test area, per illumination, and beam strength); the complete set of aggregated metric values for all the different combinations are tabulated in Appendix. Sample retrieval errors were computed for each parameter, h_te_interp, h_canopy_abs, h_canopy, and h_canopy normalized to rCH for which there were valid HDL and ATL08 values (with no outlier removal). Because ATL08 segments may exist with h_te_interp values but no h_canopy_abs h_canopy values, the number of validated segments varied for each parameter. Total values of validated segment per parameter are h_te_interp 29 145; h_canopy_abs 28 137; and h_canopy 28 230; these values and their associated error metrics are listed in Table II.

## III. Results and Discussion

For this article, multiple exploratory error analyses were performed, including correlation with terrain slope and laser penetration index (as a proxy for canopy openness) derived from the HDL; the ATL08 ICESat-2 estimated parameter uncertainties were also compared with the external validation results. However, for brevity, the results and discussion will focus on the most relevant error factors identified: the effect of the rCH on the ATL08 retrieval error of elevation of terrain (h_te_interp) and top of canopy (h_canopy_abs), and the resultant estimated canopy height (h_canopy). These results are summarized in Fig. 4, which presents box and whisker plots where the interquartile range (IQR) of the errors are represented as the box and the whiskers represent the values for the 5th and 95th percentiles for rCH groups stratified into 5-m intervals. The subplots in Fig. 4 also include a bar graph to depict the number of samples in each rCH strata. While the whiskers represent the limits of the 5th to 95th percentile for individual retrieval errors, error metrics (RMSE, MAE, etc.) were computed considering all error values.

In Figs. 1 and 4, it is observed that for dense tropical forest conditions, the errors of the ATL08-derived parameters vary widely, even within a relatively short distance in the same orbital pass and for the same sensor beam. Fig. 1 shows a profile comparing HDL reference and ATLAS retrieved elevations for terrain and top of canopy; the ATLAS observations are for a strong beam at night over medium-roughness terrain with rCHs in excess of 50 m. In this profile, the right two-thirds show relatively good agreement between ATLAS and HDL. However, the left third of the profile exhibits significant top of canopy retrieval errors despite accurate terrain retrieval; this results in significant errors in estimated canopy height (h_canopy). This is most likely due to a significant amount of photon-events produced by low atmospheric or forest transpiration obscurations (revisited in a later paragraph).

The 5th to 95th percentile error values in h_te_interp retrieval grow proportional to the rCH from $\pm 2.5$ m for areas with fairly low rCH (5–10 m) all the way to $-10$–24 m for areas with rCH of 40–45 m. The minimum and maximum h_te_interp errors are $-108.381$ and 108.37 m, respectively; these extreme values seem to be a reflection of the $\pm 120$-m buffer from a global DEM used for the classification of ATL03 photon-events [18]. The 5th to 95th percentiles and IQR shown in Fig. 4(a) display an asymmetrical error range; this indicates that much fewer photon-events are identified as terrain from below the reference terrain (underestimated) than those that are classified above the reference surface (overestimated). The median of the h_te_interp errors [Fig. 5(a)] also grows proportionally with rCH and consistently overestimates with respect to the reference; this indicates

TABLE II
OVERALL RETRIVAL ERROR METRICS—THIS AND OTHER STUDIES

| Study / Retrieved Parameter | Validation Location | Δt years | Terrain Elevation [m] # Seg / mean, RMSE, MAE | Canopy Height CH [m] # Seg / mean, RMSE, MAE | Normalized CH RMSE / MAE |
|---|---|---|---|---|---|
| Neuenschwander *et al.* [14] | Finland | ~ 0 - 11 | 909,467 / -0.07 / 0.73 / 0.53 | 582,903 / -1.47 / NR / NR | 19.54 / NR |
| Queinnec *et al.* [17] [1] | Canada, ON | | | 846 /-2.3 /2.9 / 2.0 | 23.7 / 12.5 |
| Tian & Shan [12] | USA, IN | | NR / -0.07 / 0.26[2]/ NR | NR | NR |
| | USA, CA | | NR / -0.232 / 2.29[2] /NR | NR | NR |
| Liu, Cheng & Chen [15] [3] | CONUS + AK, HI | ~ 0 - 1 | 32,666 / -0.20 / 2.24 / 0.91 | 20,967 / -0.77 / 7.21 / 4.33 | NR / NR |
| Malambo & Popescu [16] | CONUS | ~ 1 - 12 | 79, 497 / 0.18 / NR / 1.2 | 83,512 / -1.71 / NR / 3.44 | NR / 31.9[4] |
| This study | Mexico, Guatemala, Belize and Honduras | 0.4 - 8.3 | 29,484 / 3.07 / 10.58 / 4.54 | 28,369 /-1.26 / 13.35 / 6.79 | 67.0/30.9 |

$\Delta t$: absolute temporal difference between ATLAS and reference data acquisitions, #Seg: number of ATL08 samples validated per parameter and test site, RMSE: root mean square error, MAE: mean absolute error. Notes: 1. Queinnec *et al.* compare ATLAS to airborne single-photon lidar (SPL) measurements and because of the experimental nature of both they use the term "difference" instead of "error" and reports root mean square difference (RMSD) and mean absolute difference (MAD); for canopy height, they compare ATL08 canopy height vs. height of 90th percentile of the airborne SPL and the number tabulated here for normalized canopy height come from comparison of 95th percentile for both ATLAS and SPL, for top of canopy, it compares %Tot: percentage for area of total segments (29 484). BR is abbreviation for biosphere reserve, R for reserve. 2. Tian and Shan report standard deviation of the errors which numerically should be very close to the RMSE; the numbers tabulated here are for vegetated segments not overall. The values tabulated here are the reported by Liu *et al.* for mid to low latitudes not overall. 4. Reported value as percentage MAE (pMAE).

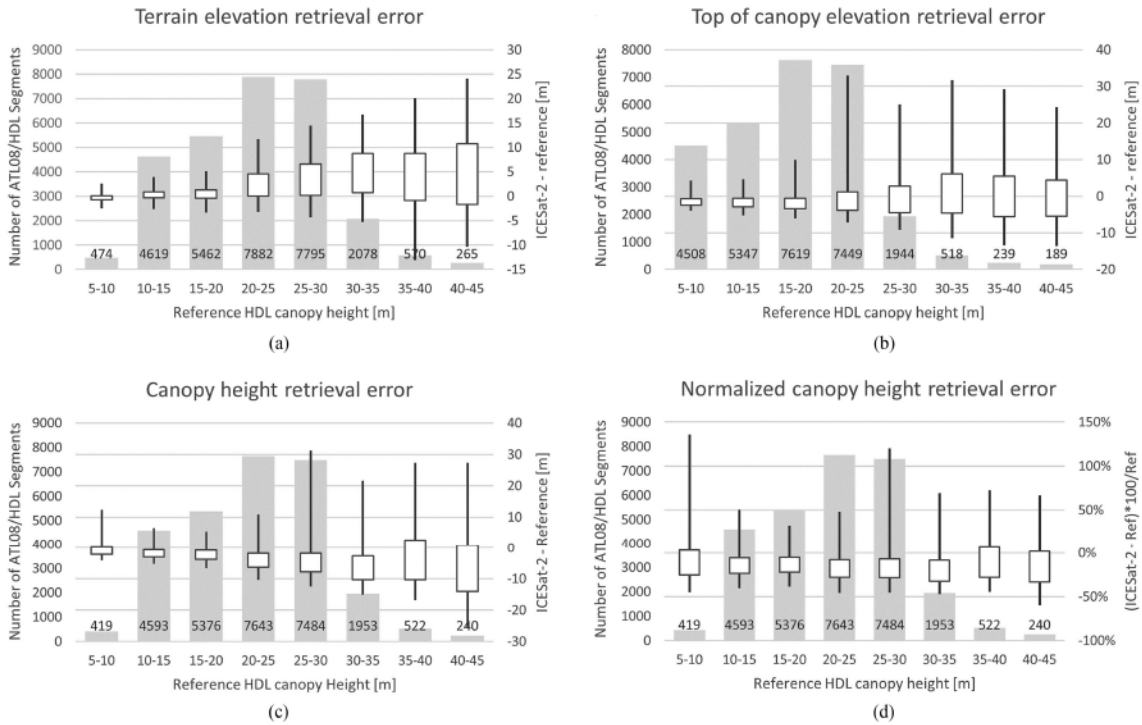


Fig. 4. Retrieval error characteristics as box and whisker plots stratified by reference canopy height (rCH) in 5-m intervals and bar graphs showing the number of available ATL08/HDL segment pairs in each rCH strata for (a) interpolated terrain elevation (h_te_interp), (b) top of canopy elevation (h_canopy_abs), (c) estimated canopy height (h_canopy), and (d) normalized % canopy height error.

that the ATLAS laser energy has difficulty penetrating all the way through the canopy to produce consistent ground photon-events. This behavior should be expected for dense high closure forests, but the corresponding behavior has not previously been observed and reported for other forests types, quite the contrary, results from other studies summarized in Table II indicate a fairly accurate retrieval of terrain for boreal and temperate forests.

With respect to h_canopy_ab [Fig. 4(b)], which is not reported in other articles, perhaps because of the difficulty generating high fidelity and accuracy top of canopy elevations from low density ALS data, it was observed that the 5th to 95th percentile error range grows with increased rCH but at a much lower rate; the IQR is generally constrained between −5.5 and 6.0 m, while the median [Fig. 5(b)] remains mostly uniform and independent of the rCH but underestimates the reference by −0.5–−2.0 m. While errors in h_canopy_ab have not been reported directly elsewhere, our error metric values are consistent in magnitude and direction with the eCH error values reported in [14], [17]; given that in the boreal forests the retrieval of terrain has been shown to be fairly accurate. This suggests that the sensor and data processing algorithms are moderately successful in detecting the

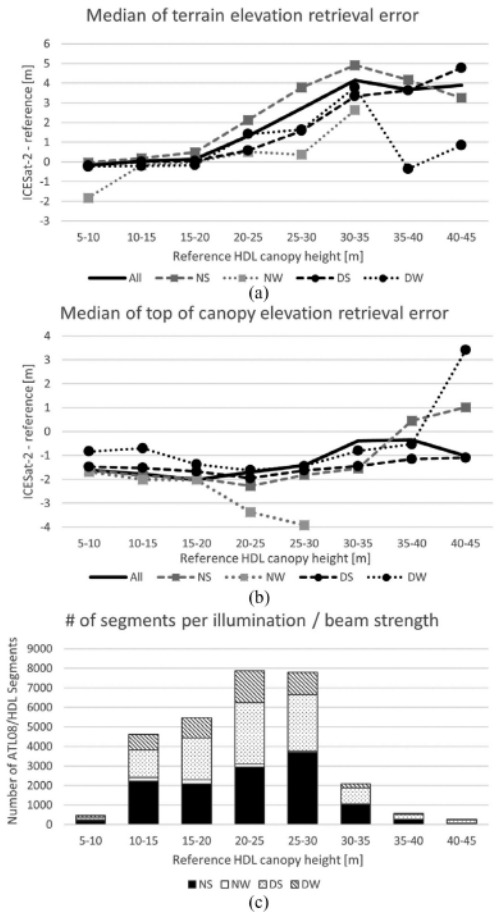


Fig. 5. Trends for the median values of the retrieval errors for (a) h_te_interp and (b) h_canopy_abs separated by day or night and weak or strong beams (NS—night and strong, NW—night and weak, DS—day and strong, and DW—day and weak); (c) bar graph showing the number of validated ATL08 segments as a function of illumination and beam strength combinations.

top of high closure tropical forest canopies. Some of the observed variation may be due to changes in the openness and roughness of the top of canopy, but an exploration and discussion of this is outside the scope of this communication.

From both an ecology and global carbon budget point of view, the most valuable metric that can be estimated from the ATLAS observations is the forest canopy height (h_canopy). h_canopy is a biophysical parameter and its value is computed through remote means as a relative measure by subtracting the elevation of the terrain from the elevation of the top of the vegetation or by *in-situ* measurement. Therefore, the validation of this measure should not be significantly influenced by differences in the geodetic reference of the satellite and airborne observations provided that the transformations between references and units are made correctly. The errors in h_canopy (meters) are presented in Fig. 4(c) and in Table II; the behavior of these errors are a combination of terrain retrieval errors and top of canopy estimation errors. As summarized in Table II, our validations report the second lowest mean h_canopy error, but the highest RMSE and MAE value. While the 5th to 95th percentile h_canopy errors oscillate between −25 and 30 m, the overall minimum and maximum values are −30.15 and 123.26 m, again reflecting the retrieval error ranges for both terrain and top of canopy.

The h_canopy errors are important, however, a more relevant metric is the ratio of that error to the rCH. This relative error provides a better sense of the scale and impact of these errors because it is normalized with respect to the natural phenomena that it is attempting to quantify. The IQR of the errors in ATL08 h_canopy normalized to the rCH exhibit a mostly uniform behavior across the range of reference CH between −33.5% and 7.0%, with the median fluctuating around an underestimation level of −16.5% and an associated RMSE% of 67.0%. While the overall median obtained in our validations is close to the best case underestimation averages of 11%–13% reported in [14], the RMSE% value is much higher than the 14.5% reported in the same study and the 23.7% RMSD in [17], both for boreal forests. Our overall h_canopy %MAE is 30.9%, very close to the 31.9% reported in [16] for temperate forests and subtropical savannahs. Again, this high variability of retrieval error is indicative of the difficulty accurately detecting the terrain under tropical forests. However, the fact that the median and IQR of the normalized canopy height errors exhibit a mostly uniform behavior [Fig. 4(d)] is the most important and potentially useful result. This uniform behavior can be used to propagate the uncertainty within any biophysical model that employs ICESat-2 derived canopy height as an input—for instance, models that attempt to estimate carbon storage in tropical forests as a function of retrieved canopy height.

The overall (all samples under all conditions) RMSE values are 10.58 m for h_te_interp, 17.18 m for h_canopy_abs, and 13.35 m for h_canopy. These values are much higher than similar error metrics reported in other studies for boreal and temperate forests (Table II), which is partially due to the much more difficult retrieval conditions presented by tropical forests, but also because we did not exclude any ATL08 data as outliers and did not dynamically displace ATL08 data to better match the HDL. We did experiment with a geolocation adjustment for approximately 25% of our samples; however, the currently available tools do not work well when the ATLAS retrieved terrain is extremely noisy with overestimated elevations. When geolocation corrections were estimated and applied, only a minuscule improvement in h_te_interp retrieval was obtained for some ATLAS profiles but not overall. At the same time, h_canopy_abs retrieval accuracy is degraded and there was no significant change in the retrieval accuracy of h_canopy (see Appendix, Table VII for the overall geolocation adjustment results and Table VIII for the per beam/pass results).

We recognize the importance of contextualizing our ICESat-2/ATLAS performance results with previous research that employed ICESat/GLAS data, particularly with studies that derived canopy heights in tropical forest such as [36] and [37]. However, this is problematic for several reasons as follows:

1) The marked differences in sensor design (footprint size and signal processing/recording approach) make the GLAS and ATLAS observations and results too disparate for direct comparison.
2) Canopy or vegetation height is not an observable in the GLAS data products. Thus, many researchers developed

a myriad of algorithms using both ancillary data, and site-specific statistical models to obtain canopy and vegetation height from the raw geolocated waveforms (GLA01), or from the different Gaussian components reported in the GLA14 (global land surface altimetry data) [38]. Of all the ICESat studies, the results most comparable to ATL08 h_canopy would be those that were derived using the direct method such as in [36], [39], [40], [41]. However, even with the direct method, there were several alternative Gaussian components used to estimate the ground surface elevation. A good review of different issues, results, and approaches taken for canopy height estimation with ICESat/ GLAS data is presented in [36].

3) The majority of the research based on the ICESat/GLAS was applied to small test areas and relatively few lidar footprints; one notable exception is [42] which produced a global canopy height map.
4) There was previously a paucity of even low-density airborne lidar available over extended regions to validate terrain, top of canopy elevations, and canopy heights from ICESat. Comparisons between HDL and ICESat-2 are more prevalent and rigorous because there is now a significant amount of openly available HDL data.

With regards to the typical overall error metrics such as MAE and RMSE, it is important to stress that they hide important error trends as a function of the rCH, which are better observed in the graphs in Figs. 4 and 5. Thus, as an additional analysis, the trends for the error medians of h_te_interp and h_canopy_abs were segregated for different illumination conditions (day or night) and beam strength (weak and strong) as done for h_canopy in most other validation studies. The possible combinations have been abbreviated and their overall distribution (for h_te_interp segments) is as follows: NS for night and strong (42.9%), NW for night and weak (2.3%), DS for day and strong (37.6%), and DW for day and weak (17.2%). The results are presented in Fig. 5, and to assist interpretation Fig. 5(c) displays a bar graph of the number of validated ATL08/HDL segments for each illumination and the strength condition in each of the rCH strata. It is important to note that no single metric by itself should be used to rank the performance of a particular beam strength and solar illumination conditions. We considered the combination of three metrics to inform the labeling of the best performing one. These metrics are the median as a measure of central tendency (median), the RMSE as a measure of dispersion, and the percentage of available segments for each combination as a function of the total number of segments.

From Fig. 5(c), it can be observed that most of the ATL08 segments validated in this article come from the strong beams for both night and day conditions, followed by weak beams during the day. The number of ATL08 segments analyzed from weak beams during the night is extremely low: about 665 segments or 2.3% of our entire validation dataset. This is indicative of the level of difficulty faced by the retrieval algorithms to separate signal from noise in these complex forests with the additional complications of significant laser obscuration due to meteorological and forest metabolic processes. While the graph in Fig. 5(a) may seem to indicate that NW has good performance for h_te_interp retrieval, the limited number of samples do not allow for a generalized conclusion.

For the following discussion, we ignore the samples for NW and the lowest and the two highest rCH strata due to the relatively low numbers of validations samples for these segregated combinations. Fig. 5(a) suggests that just based on the behavior of the median of errors throughout the range of rCH, the candidate for best performing combination for retrieval of h_te_interp is the strong beams during the day (DS) followed by DW. The strong beams during the night (NS) had the worst performance. The overall RMSE for each combination are given as DS 6.04 m, DW 5.91 m, NW 6.67 m, and NS 14.59m. These suggest slightly better performance for the DW over the DS. However, the RMSE results are very sensitive to outliers, which are more likely to be present with a higher number of samples. For h_te_interp, DS produced more than double the validated segments than DW. Overall, considering all three metrics, DS is the best performing combination. This behavior is different than the validation presented for terrain elevations in [15], where NS had the lowest RMSE of the four possible combinations and DW the highest. These results are counter to the general expectation that observations during the night should be less noisy than day observations. However, the discrepancy may be explained in the context in tropical forests, where significant laser energy is required to penetrate the forest canopies, and where during the night, high humidity and vegetation metabolism may cause additional laser obscuration phenomena [43]–[45] which may counter the benefit of low background solar radiation. An example of low altitude and partial obscuration phenomena during the night is illustrated in the left third of Fig. 1.

For the retrieval of h_canopy_abs, Fig. 5(b) illustrates that based on median alone the candidate for best performance combination is for weak beams during the day (DW) followed by strong beams during the day (DS). The overall RMSE for h_canopy_abs retrieval for the different combinations are given as DS 4.87 m, DW 5.72 m, NW 11.2 m, and NS 25.5m. This, combined with the relative number of validated ATL08/HDL segments (with DS 38.2% vs. DW 16.8%) again, suggests that DS is the best performing combination both in terms of accuracy and retrieval of ATL08 segments.

With regards to h_canopy which is subject to a combinations of the factors that affect the retrieval of h_te_interp and h_canopy_abs, our results indicate that when just considering the trend of the median against the rCH, the day and weak (DW) combination followed by day and strong (DS) are the primary candidates for best performance. Night and strong showed the worst performance. The overall RMSE are given as DS 7.19 m, DW 7.56 m, NW 7.24 m (only 584 samples), and NS 18.6m. This, and the relative number of validated ATL08/HDL segments (with DS 38.3% vs. DW 16.8%) again suggests that DS has the best performance for our validation samples.

Similar analyses examining the effect of beam strength and background illumination conditions on the retrieval of h_canopy has been performed for boreal forests in Finland and mostly temperate forests in the conterminous USA. For boreal forests, presented in [14], using summer observations and only considering strong beams (authors do not recommend using weak beams

for canopy heights retrievals), it was reported that the ATLAS observations during the day had a lower bias (mean) than those for the night; however, the dispersion (RMSE) was higher during the day by about 7 cm. In our case, the bias is also closer to zero for the night observations (0.43 m vs. −3.03 m); however, the RMSE for night observations (18.60 m) is more than double the RMSE for day observations (7.19 m). The results for the mostly temperate forests presented in [16] are only reported for aggregated strong vs. weak or day vs. night as a function of the canopy height percentile. Their results indicate lower bias during day observations but with a higher dispersion (%MAE); this is similar to the observations for boreal forests. Our data from tropical forests again indicates a lower bias during the night (0.31 vs. −2.54), but the %MAE is 21.6% for day and 42.4% during the night. With regards to beam strength, their results indicated lower bias for the weak beams but with a higher dispersion (%MAE); our experiment yielded the opposite results with a slightly lower bias for the strong beams (−1.2 m vs. −1.5 m) but also a higher dispersion (32.8% vs. 22.5%).

Although it is not possible to arrive at generalized conclusions from these conflicting assessments of beam strength and illumination conditions for the different forest environments as presented, it is possible to observe that localized environmental and forest structure conditions will cause wide variations in ATLAS sensor performance for different beam and time of day combinations. Furthermore, day versus night conditions represent an over-simplification of illumination conditions, perhaps more consistent results may be obtained by considering the angular separation between the specific ATLAS beam detector and the Sun at the footprint projection by using the solar_elevation and solar_azimuth fields contained in the ATL08 file. Continued validation of ATLAS observations for the entire sensor and spacecraft lifetime at the current and additional test sites with more detailed analysis and ancillary meteorological and atmospheric data is required to better understand and characterize different illumination and beam strength performance.

As a final point of discussion, we would like to present some recommendations to both end-users of ATL08 data in tropical regions and to the scientists looking to develop algorithms for raw ATLAS observations. The ATLAS single-photon design with extremely high sensitivity detects a large number of noise photon-events, which makes it hard to disentangle noise that is due to atmospheric (clouds and fog) or other obscurant (smoke and biotranspiration) phenomena from sensor noise for individual photon-events located near the ground and vegetation portion of the range gate. As a result, there is a wide range of errors observed for terrain (h_te_interp and h_te_mean) and top of canopy elevations (h_canopy_abs) as well as the resultant canopy height (h_canopy) and their associated uncertainties (h_te_uncertainty and h_canopy_uncertainty). These derived geophysical or biophysical parameters for individual ATL08 segments have to be utilized with reasonable caution. However, values obtained by aggregating multiple observations (temporally, spatially, and statistically) can provide reasonable data.

For this validation, we did not remove any evident outlier data in the ATL08 files. Outliers in h_canopy can be filtered-out by using local knowledge from ground measurements or airborne lidar. For instance, from our reference data, we know that canopy heights in the rain forest in Mesoamerica rarely exceed 60 m. In the absence of this local knowledge, significant differences to other independently derived canopy height models such as GFCH2019 [46] or even older models produced from ICESat/GLAS observations [42], [47] can also be used to flag potential outliers. In our analysis, we did not find a meaningful correlation between the ATL08 reported uncertainties and the externally validated errors. However, in the absence of ancillary data, a practitioner can use the reported internal uncertainties as well as other quality flags such as terrain_flg and cloud_flag_atm to filter out potentially unreliable observations.

Finally, just as a global DEM/DSM is used to limit the photon-events within a reasonable range for terrain and top of canopy retrieval for the processing of ATL03 to ATL08 products, a combination of the GLAS [42], [47] and GEDI [46] canopy height models among others could be used as a check for ATL08 reported h_canopy. It is important to recognize that GLAS and GEDI canopy height models have their own issues related to positional uncertainty and dense canopy characterization, so only large discrepancies may indicate potential processing issues for a particular ATL08 segment. Such discrepancy could be used to flag all retrieved elevations (terrain and top of canopy) and canopy heights as being potentially unreliable.

## IV. Conclusion

Validation of remotely sensed data is an important and challenging task in the geosciences. One of the more difficult tasks is condensing a wide range of performance results and influencing factors into a few metrics that are easier to comprehend and perhaps generalize. Results from other articles for boreal and temperate forests indicated a relatively small bias and some modest dispersion in the accuracy of ICESat-2 ATLAS terrain and forest canopy retrievals. The results presented here indicate a higher degree of variation reflected in higher bias and dispersion (RMSE and MAE) which yields lower accuracy in the retrieval of terrain and top of canopy elevations as well as the canopy height for tropical forest environments. This degraded performance is perhaps expected due to the single photon detection design of the ATLAS and the current stage of canopy retrieval algorithms. However, the results are also encouraging in that the top of canopy elevations can be retrieved with a fair degree of accuracy and the median of the relative errors of canopy heights seems to exhibit a uniform behavior that can be used to propagate uncertainty to models and algorithms that leverage canopy data. Despite the overall low accuracy of ATLAS biophysical parameter retrievals in tropical forests, averaged or aggregated values can still provide important insight regarding forest structure for remote areas where *in-situ* or even airborne remote sensing observations are not feasible. Further research with validation, more discussions regarding the methodology of validation, better understanding of the sensor characteristics, and new or refined retrieval algorithm development can improve the quality of the ATLAS derived data in tropical forests.

## APPENDIX
## BREAKDOWN VALIDATION AND GEOCORRECTION RESULTS

Abbreviations used in the following tables: OP/BT—number of orbital passes and beam tracks assesed, #Seg—number of ATL08 segments (100 m) validated, RMSE—root mean square error, $R^2$—coefficient of determination, Min—minimum, Max—Maximum, Std—standard deviation, MAE—mean absolute error, nRMSE—Normalized RMSE, nMAE—normalized MAE, nMean—normalized mean, GTMBR—Maya Biosphere Reserve in Guatemala, MXPuuc—Puuc Region in Mexico, GTLcnd—Lacandon region in Guatemala, MXCoba—Coba region in Mexico, MXCalak—Calakmul Biosphere Reserve in Mexico, BZRBrv—Rio Bravo Reserve in Belize, HNRPl—Rio Platano Reserve in Honduras.

TABLE III
TERRAIN ELEVATION (H_TE_INTERP) RETRIEVAL ERROR—AGGREGATED ERROR METRICS

| Evaluation set | # OP/BT | # Seg | RMSE | $R^2$ | Min | Max | Mean | Std | MAE | Median |
|---|---|---|---|---|---|---|---|---|---|---|
| Overall | 187 | 29484 | 10.59 | 0.99 | -108.38 | 108.37 | 3.07 | 10.13 | 4.55 | 0.88 |
| Night | 82 | 13359 | 14.28 | 0.98 | -33.79 | 108.37 | 5.32 | 13.25 | 6.05 | 1.55 |
| Day | 105 | 16125 | 6.00 | 1.00 | -108.38 | 99.65 | 1.21 | 5.88 | 3.31 | 0.37 |
| Strong | 121 | 23731 | 11.42 | 0.98 | -108.38 | 108.37 | 3.65 | 10.82 | 4.85 | 1.07 |
| Weak | 66 | 5753 | 6.01 | 1.00 | -105.77 | 77.00 | 0.66 | 5.97 | 3.28 | 0.19 |
| NS | 58 | 12649 | 14.59 | 0.98 | -33.79 | 108.37 | 5.58 | 13.48 | 6.26 | 1.69 |
| NW | 24 | 710 | 6.67 | 1.00 | -16.09 | 64.33 | 0.64 | 6.64 | 2.31 | -0.03 |
| DS | 63 | 11082 | 6.04 | 1.00 | -108.38 | 99.65 | 1.46 | 5.86 | 3.25 | 0.39 |
| DW | 42 | 5043 | 5.91 | 0.99 | -105.77 | 77.00 | 0.67 | 5.87 | 3.42 | 0.29 |
| GTMBR | 59 | 20353 | 12.10 | 0.91 | -108.38 | 108.37 | 4.17 | 11.36 | 5.35 | 1.51 |
| MXPuuc | 20 | 1431 | 4.02 | 0.93 | -23.40 | 9.54 | -0.96 | 3.91 | 2.17 | -0.11 |
| GTLcnd | 19 | 895 | 11.05 | 0.95 | -33.79 | 98.43 | 3.28 | 10.56 | 5.83 | 1.67 |
| MXCoba | 9 | 543 | 2.15 | 0.68 | -6.57 | 8.44 | 0.15 | 2.15 | 1.22 | -0.22 |
| MXCalak | 31 | 3816 | 2.92 | 0.92 | -103.03 | 65.75 | 0.63 | 2.85 | 1.37 | 0.02 |
| BZRBrv | 33 | 1842 | 4.66 | 0.99 | -78.09 | 40.58 | 0.10 | 4.66 | 2.90 | -0.65 |
| HNRPl | 16 | 604 | 13.93 | 0.95 | -105.77 | 99.65 | 2.26 | 13.76 | 9.18 | 2.23 |

TABLE IV
TERRAIN ELEVATION (H_TE_INTERP) RETRIEVAL ERROR FOR UN-VEGETATED SEGMENTS—AGGREGATED ERROR METRICS

| Evaluation set | # OP/BT | # Seg | RMSE | $R^2$ | Min | Max | Mean | Std | MAE | Median |
|---|---|---|---|---|---|---|---|---|---|---|
| Overall | 187 | 102 | 1.95 | 1.00 | -3.87 | 9.97 | -0.62 | 1.86 | 1.16 | -0.26 |
| Night | 82 | 62 | 2.27 | 1.00 | -3.14 | 9.97 | -0.53 | 2.23 | 1.39 | -0.67 |
| Day | 105 | 40 | 1.30 | 1.00 | -3.87 | 0.37 | -0.76 | 1.07 | 0.80 | -0.26 |
| Strong | 121 | 82 | 2.04 | 1.00 | -3.87 | 9.97 | -0.54 | 1.98 | 1.19 | -0.29 |
| Weak | 66 | 20 | 1.57 | 1.00 | -3.80 | 0.16 | -0.96 | 1.27 | 1.05 | -0.14 |
| NS | 58 | 45 | 2.52 | 1.00 | -2.38 | 9.97 | -0.39 | 2.52 | 1.54 | -1.48 |
| NW | 24 | 17 | 1.43 | 1.00 | -3.14 | 0.16 | -0.89 | 1.15 | 0.99 | -0.06 |
| DS | 63 | 37 | 1.20 | 1.00 | -3.87 | 0.37 | -0.71 | 0.98 | 0.76 | -0.29 |
| DW | 42 | 3 | 2.20 | 1.00 | -3.80 | -0.13 | -1.36 | 2.12 | 1.36 | -0.14 |
| GTMBR | 59 | 13 | 1.51 | 1.00 | -3.87 | 0.14 | -0.62 | 1.43 | 0.68 | -0.09 |
| MXPuuc | 20 | 8 | 0.80 | 0.98 | -0.08 | 1.41 | 0.62 | 0.53 | 0.64 | 0.49 |
| GTLcnd | 19 | 41 | 2.22 | 0.95 | -1.25 | 9.97 | 0.42 | 2.20 | 0.66 | 0.02 |
| MXCoba | 9 | - | - | - | - | - | - | - | - | - |
| MXCalak | 31 | - | - | - | - | - | - | - | - | - |
| BZRBrv | 33 | 40 | 1.95 | 1.00 | -3.14 | -1.40 | -1.93 | 0.30 | 1.93 | -1.89 |
| HNRPl | 16 | - | - | - | - | - | - | - | - | - |

TABLE V
TOP OF CANOPY ELEVATION (H_CANOPY_ABS) RETRIEVAL ERROR—AGGREGATED ERROR METRICS

| Evaluation set | # OP/BT | # Seg | RMSE | $R^2$ | Min | Max | Mean | Std | MAE | Median |
|---|---|---|---|---|---|---|---|---|---|---|
| Overall | 187 | 28137 | 17.18 | 0.97 | -29.74 | 134.26 | 1.67 | 17.10 | 6.02 | -1.76 |
| Night | 82 | 12601 | 25.04 | 0.94 | -29.74 | 134.26 | 4.93 | 24.55 | 9.58 | -1.94 |
| Day | 105 | 15536 | 5.15 | 1.00 | -26.70 | 91.85 | -0.99 | 5.05 | 3.13 | -1.59 |
| Strong | 121 | 22809 | 18.82 | 0.96 | -29.74 | 134.26 | 2.21 | 18.69 | 6.66 | -1.82 |
| Weak | 66 | 5328 | 6.55 | 0.99 | -24.06 | 112.43 | -0.65 | 6.51 | 3.27 | -1.43 |
| NS | 58 | 12021 | 25.51 | 0.94 | -29.74 | 134.26 | 5.24 | 24.97 | 9.85 | -1.92 |
| NW | 24 | 580 | 11.22 | 0.99 | -20.04 | 112.43 | -1.46 | 11.14 | 3.96 | -2.26 |
| DS | 63 | 10788 | 4.87 | 1.00 | -26.70 | 85.99 | -1.18 | 4.73 | 3.10 | -1.71 |
| DW | 42 | 4748 | 5.72 | 0.99 | -24.06 | 91.85 | -0.55 | 5.69 | 3.19 | -1.26 |
| GTMBR | 59 | 19452 | 20.03 | 0.81 | -24.06 | 134.26 | 2.75 | 19.84 | 7.03 | -1.81 |
| MXPuuc | 20 | 1403 | 4.61 | 0.94 | -19.33 | 28.89 | 0.14 | 4.61 | 3.11 | -0.99 |
| GTLcnd | 19 | 757 | 15.60 | 0.91 | -23.62 | 118.76 | 1.99 | 15.48 | 8.19 | -1.66 |
| MXCoba | 9 | 531 | 2.57 | 0.46 | -13.39 | 4.52 | -1.82 | 1.81 | 2.01 | -1.65 |
| MXCalak | 31 | 3806 | 3.13 | 0.92 | -8.22 | 77.85 | -1.13 | 2.92 | 1.87 | -1.52 |
| BZRBrv | 33 | 1643 | 7.48 | 0.98 | -29.74 | 85.99 | -3.30 | 6.71 | 5.19 | -4.08 |
| HNRPl | 16 | 545 | 17.10 | 0.93 | -26.70 | 97.44 | 4.24 | 16.58 | 9.58 | 0.67 |

TABLE VI
CANOPY HEIGHT (H_CANOPY) RETRIEVAL ERROR—AGGREGATED ERROR METRICS

| Evaluation set | # OP/BT | # Seg | RMSE | $R^2$ | Min | Max | Mean | Std | MAE | Median | nRMSE | nMAE | nMean |
|---|---|---|---|---|---|---|---|---|---|---|---|---|---|
| Overall | 187 | 28369 | 13.36 | 0.16 | -30.15 | 123.26 | -1.26 | 13.30 | 6.80 | -3.18 | 0.67 | 0.31 | -0.05 |
| Night | 82 | 12706 | 18.23 | 0.13 | -26.06 | 120.20 | 0.31 | 18.23 | 9.34 | -3.84 | 0.92 | 0.42 | 0.02 |
| Day | 105 | 15663 | 7.31 | 0.26 | -30.15 | 123.26 | -2.54 | 6.86 | 4.73 | -2.65 | 0.36 | 0.22 | -0.10 |
| Strong | 121 | 23005 | 14.38 | 0.15 | -30.15 | 120.20 | -1.21 | 14.33 | 7.31 | -3.39 | 0.72 | 0.33 | -0.04 |
| Weak | 66 | 5364 | 7.53 | 0.29 | -23.95 | 123.26 | -1.51 | 7.38 | 4.61 | -2.10 | 0.38 | 0.22 | -0.06 |
| NS | 58 | 12122 | 18.60 | 0.12 | -26.06 | 120.20 | 0.44 | 18.59 | 9.60 | -3.93 | 0.94 | 0.43 | 0.03 |
| NW | 24 | 584 | 7.24 | 0.20 | -23.95 | 69.51 | -2.36 | 6.85 | 4.08 | -2.60 | 0.38 | 0.23 | -0.13 |
| DS | 63 | 10883 | 7.19 | 0.25 | -30.15 | 100.84 | -3.04 | 6.52 | 4.75 | -2.86 | 0.35 | 0.21 | -0.12 |
| DW | 42 | 4780 | 7.57 | 0.28 | -19.98 | 123.26 | -1.40 | 7.44 | 4.67 | -1.99 | 0.38 | 0.22 | -0.47 |
| GTMBR | 59 | 19480 | 15.31 | 0.06 | -21.22 | 123.26 | -1.02 | 15.28 | 7.82 | -3.76 | 0.72 | 0.34 | -0.03 |
| MXPuuc | 20 | 1442 | 5.19 | 0.12 | -18.38 | 41.79 | 0.45 | 5.18 | 3.34 | -1.02 | 0.61 | 0.26 | 0.06 |
| GTLcnd | 19 | 784 | 12.47 | -0.03 | -27.79 | 62.96 | -2.62 | 12.20 | 9.38 | -5.27 | 1.25 | 0.40 | 0.04 |
| MXCoba | 9 | 541 | 3.23 | -0.14 | -13.10 | 9.31 | -1.89 | 2.61 | 2.48 | -1.74 | 0.20 | 0.16 | -0.12 |
| M MXCalak | 31 | 3873 | 3.78 | 0.09 | -9.38 | 76.25 | -1.91 | 3.26 | 2.62 | -1.99 | 0.27 | 0.19 | -0.14 |
| BZRBrv | 33 | 1678 | 8.60 | 0.02 | -26.06 | 94.62 | -4.00 | 7.62 | 6.04 | -4.59 | 0.55 | 0.30 | -0.13 |
| HNRPl | 16 | 571 | 16.20 | -0.08 | -30.15 | 109.83 | 0.85 | 16.19 | 11.47 | -2.16 | 0.49 | 0.31 | 0.05 |

TABLE VII
OVERALL AGGREGATED ERROR METRICS FOR H_TE_INTERP, H_CANOPY_ABS, AND H_CANOPY RETRIEVALS AS PRODUCED AND REPORTED IN ATL08 FILES AND AFTER AN ATTEMPT OF GEOLOCATION ADJUSTMENT USING PHOREAL

| . | h_te_interp | | | h_canopy_abs | | | h_canopy | | |
|---|---|---|---|---|---|---|---|---|---|
| | # Seg | RMSE | MAE | # Seg | RMSE | MAE | # Seg | RMSE | MAE |
| As produced | 7312 | 5.83 | 3.51 | 7188 | 5.61 | 3.45 | 7239 | 7.65 | 5.51 |
| XYZ shifted | 7309 | 6.32 | 4.16 | 7188 | 8.61 | 6.94 | 7239 | 7.66 | 5.53 |
| XY-only shifted | 7309 | 5.84 | 3.51 | 7188 | 5.66 | 3.51 | 7239 | 7.66 | 5.53 |

The error metrics for "As produced" correspond to the values reported in the ATL08 files without any correction, "*XYZ* shifted" are the resultant overall error metrics when the recommended shifts are applied in the UTM three dimensions, and "*XY*-only shifted when the correction in *Z* is ignored.

TABLE VIII
PER ORBITAL PASS/BEAM AGGREGATED ERROR METRICS FOR H_TE_INTERP, H_CANOPY_ABS, AND H_CANOPY RETRIEVALS AS REPORTED IN ATL08 FILES AND AFTER AN ATTEMPT OF GEOLOCATION ADJUSTMENT USING PHOREAL

| Filename | Recommended PhoREAL shifts | | | | | h_te_interp | | | | h_canopy_abs | | | | h_canopy | | | |
|---|---|---|---|---|---|---|---|---|---|---|---|---|---|---|---|---|---|
| TestArea_Beam_ATL08File | sE | sN | sZ | xT | aT | # Seg | RMSE | DME | MAE | # Seg | RMSE | DME | MAE | # Seg | RMSE | DME | MAE |
| 01_gt1l_20190727_0454_3 | | | | | | 382 | 6.84 | 4.53 | 5.16 | 378 | 3.98 | -0.87 | 2.97 | 378 | 7.89 | -6.15 | 6.58 |
| 01_gt1l_20190727_0454_3s | 3.1 | -8.4 | -5.6 | -4 | 8 | 381 | **5.25** | -0.97 | **4.30** | 378 | ***7.51*** | -6.39 | ***6.88*** | 378 | 7.90 | -6.16 | 6.58 |
| 01_gt1l_20190727_0454_3s0 | 3.1 | -8.4 | 0 | | | 381 | 6.93 | 4.63 | 5.20 | 378 | 4.02 | -0.79 | 3.00 | 378 | 7.90 | -6.16 | 6.58 |
| 01_gt2l_20190727_0454_3 | | | | | | 396 | 6.83 | 4.22 | 4.92 | 394 | 4.20 | -0.18 | 3.13 | 396 | 7.36 | -5.19 | 5.93 |
| 01_gt2l_20190727_0454_3s | 1.3 | -6.2 | -6.6 | -2 | 6 | 397 | **5.96** | -2.27 | 4.96 | 395 | ***7.96*** | -6.66 | ***7.29*** | 396 | 7.34 | -5.18 | 5.91 |
| 01_gt2l_20190727_0454_3s0 | 1.3 | -6.2 | 0 | | | 397 | 7.00 | 4.33 | 5.03 | 395 | 4.36 | -0.06 | 3.20 | 396 | 7.34 | -5.18 | 5.91 |
| 01_gt3l_20190727_0454_3 | | | | | | 538 | 5.64 | 3.75 | 4.12 | 538 | 3.22 | -1.21 | 2.54 | 539 | 6.78 | -5.53 | 5.68 |
| 01_gt3l_20190727_0454_3s | -6 | 0.7 | -4.7 | 6 | 0 | 538 | **4.27** | -0.96 | **3.50** | 538 | ***6.61*** | -5.91 | ***6.16*** | 539 | 6.79 | -5.51 | 5.66 |
| 01_gt3l_20190727_0454_3s0 | -6 | 0.7 | 0 | | | 538 | 5.59 | 3.74 | 4.07 | 538 | 3.21 | -1.21 | 2.53 | 539 | 6.79 | -5.51 | 5.66 |
| 01_gt1r_20200421_0401_3 | | | | | | 522 | 5.62 | 2.11 | 3.86 | 509 | 5.70 | 0.28 | 3.90 | 509 | 6.68 | -2.34 | 4.96 |
| 01_gt1r_20200421_0401_3s | -2.7 | 7.8 | -7.8 | -2 | 8 | 521 | ***7.72*** | -5.67 | ***6.62*** | 508 | ***9.55*** | -7.64 | ***8.68*** | 509 | 6.73 | -2.47 | 5.02 |
| 01_gt1r_20200421_0401_3s0 | -2.7 | 7.8 | 0 | | | 521 | 5.65 | 2.13 | 3.89 | 508 | 5.73 | 0.16 | 3.98 | 509 | 6.73 | -2.47 | 5.02 |
| 01_gt2r_20200421_0401_3 | | | | | | 394 | 12.31 | -0.96 | 5.16 | 382 | 5.40 | -0.70 | 3.71 | 382 | 13.54 | -0.59 | 6.39 |
| 01_gt2r_20200421_0401_3s | -1.1 | -10.1 | -5.7 | -2 | -10 | 394 | ***14.01*** | -6.61 | ***7.82*** | 382 | ***8.33*** | -6.26 | ***7.29*** | 382 | 13.53 | -0.53 | 6.38 |
| 01_gt2r_20200421_0401_3s0 | -1.1 | -10.1 | 0 | | | 394 | 12.39 | -0.91 | 5.24 | 382 | 5.52 | -0.56 | 3.77 | 382 | 13.53 | -0.53 | 6.38 |
| 01_gt3r_20200421_0401_3 | | | | | | 384 | 4.92 | 2.09 | 3.22 | 382 | 3.54 | -1.13 | 2.66 | 383 | 5.54 | -3.69 | 4.06 |
| 01_gt3r_20200421_0401_3s | -4.6 | -16.5 | -7.9 | -6 | -16 | 384 | ***7.34*** | -5.79 | ***6.64*** | 382 | ***9.76*** | -9.06 | ***9.31*** | 382 | ***5.63*** | -3.74 | ***4.14*** |
| 01_gt3r_20200421_0401_3s0 | -4.6 | -17 | | | | 384 | 4.98 | 2.11 | 3.24 | 382 | 3.80 | -1.16 | 2.79 | 382 | 5.63 | -3.74 | 4.14 |
| 01_gt1l_20200725_0454_3 | | | | | | 714 | 5.59 | 3.82 | 4.26 | 708 | 4.13 | -1.56 | 3.28 | 708 | 7.48 | -6.34 | 6.60 |
| 01_gt1l_20200725_0454_3s | 1.8 | -2.2 | -5.4 | -2 | 2* | 713 | **4.35** | -1.54 | **3.60** | 708 | ***7.91*** | -6.92 | ***7.27*** | 709 | 7.49 | -6.35 | 6.60 |
| 01_gt1l_20200725_0454_3s0 | 1.8 | -2.2 | 0 | | | 713 | 5.61 | 3.86 | 4.27 | 708 | 4.11 | -1.52 | 3.26 | 709 | 7.49 | -6.35 | 6.60 |
| 01_gt2l_20200725_0454_3 | | | | | | 736 | 5.31 | 3.19 | 3.77 | 716 | 4.04 | -1.80 | 3.27 | 717 | 7.03 | -5.78 | 6.06 |
| 01_gt2l_20200725_0454_3s | -3.1 | 8.4 | -6.9 | 4 | -8* | 736 | ***5.72*** | -3.82 | ***4.86*** | 716 | ***9.60*** | -8.87 | ***9.06*** | 718 | ***7.09*** | -5.85 | ***6.11*** |
| 01_gt2l_20200725_0454_3s0 | -3.1 | 8.4 | 0 | | | 736 | 5.25 | 3.08 | 3.76 | 716 | 4.16 | -1.97 | 3.36 | 718 | 7.09 | -5.85 | 6.11 |
| 01_gt3l_20200725_0454_3 | | | | | | 658 | 4.83 | 3.27 | 3.66 | 654 | 3.65 | -2.19 | 2.98 | 655 | 6.84 | -5.90 | 6.10 |
| 01_gt3l_20200725_0454_3s | -5.7 | 2.7 | -4.4 | 6 | -2* | 658 | **3.73** | -1.13 | **3.00** | 654 | ***7.24*** | -6.60 | ***6.79*** | 654 | 6.81 | -5.91 | 6.10 |
| 01_gt3l_20200725_0454_3s0 | -5.7 | 2.7 | 0 | | | 658 | 4.83 | 3.27 | 3.66 | 654 | 3.70 | -2.20 | 3.01 | 654 | 6.81 | -5.91 | 6.10 |
| 02_gt2r_20200125_0454_3 | | | | | | 119 | 3.32 | -0.73 | 1.29 | 117 | 3.99 | -1.56 | 3.11 | 120 | 3.32 | -1.71 | 2.66 |
| 02_gt2r_20200125_0454_3s | 4 | -0.5 | 0.1 | -4 | 0 | 119 | **3.08** | -0.57 | **1.15** | 117 | 3.87 | -1.40 | 3.02 | 120 | 3.36 | -1.72 | 2.69 |
| 02_gt3r_20200125_0454_3 | | | | | | 131 | 2.30 | -0.49 | 1.15 | 131 | 7.56 | 2.20 | 4.79 | 133 | 7.39 | 1.73 | 4.48 |
| 02_gt3r_20200125_0454_3s | 0.5 | 0.4 | 0.1 | 0 | -4 | 131 | 2.28 | -0.38 | 1.12 | 131 | 7.58 | 2.31 | 4.78 | 133 | 7.38 | 1.74 | **4.47** |
| 02_gt1r_20190920_1285_3 | | | | | | 185 | 3.09 | -0.17 | 1.57 | 183 | 3.85 | -0.53 | 2.65 | 185 | 4.52 | -0.95 | 3.04 |
| 02_gt1r_20190920_1285_3s | 0 | 0 | 0 | 0* | 0 | 185 | 3.09 | -0.17 | 1.57 | 183 | 3.85 | -0.53 | 2.65 | 185 | 4.52 | -0.95 | 3.04 |
| 02_gt2r_20190920_1285_3 | | | | | | 130 | 2.93 | -0.06 | 1.59 | 127 | 3.86 | -0.26 | 2.78 | 130 | 3.79 | -0.75 | 2.80 |
| 02_gt2r_20190920_1285_3s | -4 | -0.3 | 0 | -4* | 0 | 130 | **2.81** | -0.08 | **1.57** | 127 | **3.77** | -0.27 | **2.77** | 130 | 3.74 | -0.75 | 2.81 |
| 02_gt3r_20190920_1285_3 | | | | | | 70 | 1.39 | 0.07 | 0.74 | 66 | 3.61 | -1.88 | 2.81 | 67 | 4.19 | -2.45 | 3.20 |
| 02_gt3r_20190920_1285_3s | 6.6 | -7.5 | 0 | 6* | -8 | 69 | ***1.53*** | -0.11 | **0.68** | 66 | **3.53** | -1.96 | **2.72** | 67 | **4.08** | -2.39 | 3.14 |

TABLE VIII
(CONTINUED)

| Filename | Recommended PhoREAL shifts | | | | | h_te_interp | | | | h_canopy_abs | | | | h_canopy | | | |
|---|---|---|---|---|---|---|---|---|---|---|---|---|---|---|---|---|---|
| TestArea_Beam_ATL08File | sE | sN | sZ | xT | aT | # Seg | RMSE | DME | MAE | # Seg | RMSE | DME | MAE | # Seg | RMSE | DME | MAE |
| 05_gt1r_20181028_0454_3 | | | | | | 227 | 3.09 | 2.52 | 2.56 | 227 | 1.80 | -1.36 | 1.58 | 228 | 4.37 | -3.99 | 3.99 |
| 05_gt1r_20181028_0454_3s | -0.6 | 12.1 | -2.8 | 2* | -12* | 227 | **1.81** | -0.31 | **1.48** | 227 | ***4.45*** | -4.24 | ***4.29*** | 227 | 4.42 | -4.03 | 4.03 |
| 05_gt1r_20181028_0454_3s0 | -0.6 | 12.1 | 0 | | | 227 | 3.07 | 2.49 | 2.57 | 227 | 1.99 | -1.44 | 1.73 | 227 | 4.42 | -4.03 | 4.03 |
| 05_gt2r_20181028_0454_3 | | | | | | 141 | 3.77 | 3.06 | 3.13 | 141 | 1.98 | -1.21 | 1.63 | 142 | 4.86 | -4.42 | 4.44 |
| 05_gt2r_20181028_0454_3s | 16.3 | -34.1 | -3.1 | -20* | 32* | 141 | **2.32** | -0.44 | **1.85** | 141 | ***5.18*** | -4.84 | ***4.90*** | 143 | **4.97** | -4.55 | **4.58** |
| 05_gt2r_20181028_0454_3s0 | 16.3 | -34.1 | 0 | | | 141 | 3.50 | 2.66 | 2.91 | 141 | 2.53 | -1.74 | 2.17 | 143 | 4.97 | -4.55 | 4.58 |
| 05_gt3r_20181028_0454_3 | | | | | | 81 | 3.81 | 3.30 | 3.35 | 81 | 1.87 | -0.72 | 1.54 | 84 | 5.00 | -4.61 | 4.62 |
| 05_gt3r_20181028_0454_3s | -13.3 | -10.6 | -3.6 | 12* | 12* | 80 | **1.97** | -0.40 | **1.57** | 80 | ***4.92*** | -4.48 | ***4.57*** | 84 | 5.01 | -4.57 | 4.65 |
| 05_gt3r_20181028_0454_3s0 | -13.3 | -10.6 | 0 | | | 80 | 3.73 | 3.20 | 3.32 | 80 | 2.22 | -0.88 | 1.81 | 84 | 5.01 | -4.57 | 4.65 |
| 05_gt1l_20190127_0454_3 | | | | | | 168 | 1.12 | 0.43 | 0.63 | 167 | 2.07 | -1.74 | 1.88 | 169 | 2.56 | -2.18 | 2.31 |
| 05_gt1l_20190127_0454_3s | 0.2 | 2 | 0.1 | 0 | -2 | 168 | 1.17 | 0.54 | 0.65 | 167 | **1.98** | -1.64 | **1.78** | 169 | 2.56 | -2.18 | 2.31 |
| 05_gt1l_20190127_0454_3s0 | 0.2 | 2 | | | | 168 | 1.13 | 0.44 | 0.63 | 167 | 2.07 | -1.74 | 1.87 | 169 | 2.56 | -2.18 | 2.31 |
| 05_gt2l_20190127_0454_3 | | | | | | 262 | 1.05 | 0.26 | 0.58 | 262 | 3.19 | -0.96 | 2.36 | 263 | 3.22 | -1.52 | 2.56 |
| 05_gt2l_20190127_0454_3s | 2 | -0.2 | 0.2 | -2* | 0* | 262 | 1.12 | 0.46 | 0.59 | 262 | **3.13** | -0.74 | **2.22** | 263 | 3.21 | -1.51 | 2.55 |
| 05_gt2l_20190127_0454_3s0 | 2 | -0.2 | 0 | | | 262 | 1.05 | 0.26 | 0.58 | 262 | 3.18 | -0.94 | 2.35 | 263 | 3.21 | -1.51 | 2.55 |
| 05_gt3l_20190127_0454_3 | | | | | | 181 | 0.93 | -0.18 | 0.46 | 181 | 2.16 | -1.67 | 1.94 | 188 | 2.28 | -1.88 | 2.05 |
| 05_gt3l_20190127_0454_3s | 0.2 | 2 | 0.2 | 0 | -2 | 181 | **0.92** | 0.02 | **0.43** | 181 | **2.02** | -1.48 | **1.78** | 188 | 2.29 | -1.89 | 2.06 |
| 05_gt3l_20190127_0454_3s0 | 0.2 | 2 | 0 | | | 181 | 0.94 | -0.18 | 0.46 | 181 | 2.17 | -1.68 | 1.95 | 188 | 2.29 | -1.89 | 2.06 |
| 06_gt1r_20191019_0340_3 | | | | | | 96 | 4.68 | 0.90 | 3.10 | 96 | 5.53 | -4.18 | 4.87 | 99 | 6.98 | -5.43 | 6.17 |
| 06_gt1r_20191019_0340_3s | 0 | 0 | -11.9 | 0* | 0 | 96 | ***11.92*** | -11.00 | ***11.17*** | 96 | ***16.48*** | -16.08 | ***16.08*** | 99 | 6.98 | -5.43 | 6.17 |
| 06_gt1r_20191019_0340_3s0 | 0 | 0 | 0 | | | 96 | 4.68 | 0.90 | 3.10 | 96 | 5.53 | -4.18 | 4.87 | 99 | 6.98 | -5.43 | 6.17 |
| 06_gt2r_20191019_0340_3 | | | | | | 103 | 4.66 | 0.26 | 2.64 | 100 | 5.92 | -4.63 | 5.22 | 102 | 7.55 | -4.86 | 6.51 |
| 06_gt2r_20191019_0340_3s | -0.4 | 4 | -9.8 | 0* | 4 | 103 | ***10.66*** | -9.60 | ***9.82*** | 100 | ***15.20*** | -14.75 | ***14.76*** | 102 | ***7.83*** | -5.11 | ***6.76*** |
| 06_gt2r_20191019_0340_3s0 | -0.4 | 4 | **0** | | | 103 | 4.64 | 0.20 | 2.65 | 100 | 6.17 | -4.95 | 5.46 | 102 | 7.83 | -5.11 | 6.76 |
| 06_gt3r_20191019_0340_3 | | | | | | 110 | 4.42 | 1.31 | 2.97 | 109 | 5.37 | -4.03 | 4.80 | 111 | 6.58 | -5.73 | 5.90 |
| 06_gt3r_20191019_0340_3s | 11.5 | 5.2 | -10.7 | 12* | 4 | 110 | ***10.62*** | -9.71 | *9.80* | 109 | **15.33** | -14.94 | **15.03** | 111 | **6.48** | -5.63 | **5.78** |
| 06_gt3r_20191019_0340_3s0 | 11.5 | 5.2 | 0 | | | 110 | 4.42 | 0.99 | 2.90 | 109 | 5.47 | -4.24 | 4.90 | 111 | 6.48 | -5.63 | 5.78 |
| 06_gt1l_20200721_0393_3 | | | | | | 90 | 2.83 | -1.04 | 2.42 | 60 | 6.72 | -5.75 | 5.95 | 61 | 7.10 | -5.72 | 6.12 |
| 06_gt1l_20200721_0393_3s | -11.9 | 1.3 | 2.2 | 12* | 0 | 90 | **2.67** | 1.03 | **1.45** | 60 | **5.55** | -3.91 | **4.54** | 61 | ***7.41*** | -5.88 | ***6.41*** |
| 06_gt1l_20200721_0393_3s0 | -11.9 | 1.3 | 0 | | | 90 | 2.73 | -1.17 | 2.38 | 60 | 7.27 | -6.11 | 6.33 | 61 | 7.41 | -5.88 | 6.41 |
| 06_gt2l_20200721_0393_3 | | | | | | 108 | 2.55 | -0.32 | 1.77 | 100 | 8.57 | -6.42 | 6.65 | 101 | 8.55 | -6.87 | 6.88 |
| 06_gt2l_20200721_0393_3s | -5.5 | 4.6 | 1.6 | 6* | -4 | 108 | ***2.96*** | 1.16 | ***1.85*** | 100 | **7.42** | -4.86 | **5.27** | 101 | 8.55 | -6.79 | **6.79** |
| 06_gt2l_20200721_0393_3s0 | -5.5 | 4.6 | 0 | | | 108 | 2.76 | -0.44 | 1.84 | 100 | 8.56 | -6.46 | 6.67 | 101 | 8.55 | -6.79 | 6.79 |
| 06_gt3l_20200721_0393_3 | | | | | | 125 | 3.52 | 1.22 | 2.39 | 123 | 5.43 | -4.24 | 4.87 | 126 | 7.55 | -6.03 | 6.69 |
| 06_gt3l_20200721_0393_3s | -9.5 | 5.1 | 1.2 | 10* | -4 | 126 | ***4.12*** | 2.28 | ***2.72*** | 124 | **4.66** | -3.11 | **4.05** | 126 | **7.39** | -5.96 | 6.65 |
| 06_gt3l_20200721_0393_3s0 | -9.5 | 5.1 | 0 | | | 126 | 3.60 | 1.08 | 2.42 | 124 | 5.53 | -4.31 | 4.91 | 126 | 7.39 | -5.96 | 6.65 |
| 08_gt1r_20181102_0530_3 | | | | | | 107 | 11.74 | 2.91 | 7.53 | 104 | 29.50 | 14.86 | 19.61 | 105 | 23.98 | 9.21 | 17.14 |
| 08_gt1r_20181102_0530_3s | -2 | 0.2 | -2.5 | 2 | 0 | 107 | **11.42** | 0.29 | **7.47** | 104 | **28.28** | 12.31 | **19.17** | 105 | 23.99 | 9.29 | 17.15 |
| 08_gt1r_20181102_0530_3s0 | -2 | 0.2 | 0 | | | 107 | 11.75 | 2.79 | 7.61 | 104 | 29.46 | 14.81 | 19.63 | 105 | 23.99 | 9.29 | 17.15 |
| 08_gt2r_20181102_0530_3 | | | | | | 10 | 9.02 | -1.38 | 6.09 | 10 | 8.77 | 1.89 | 6.57 | 14 | 10.98 | 0.36 | 9.44 |
| 08_gt2r_20181102_0530_3s | -0.4 | -4 | -2.8 | 0 | 4 | 10 | ***10.48*** | -4.85 | ***6.55*** | 10 | ***8.58*** | -1.59 | ***7.40*** | 14 | **11.10** | 0.50 | **9.29** |
| 08_gt2r_20181102_0530_3s0 | -0.4 | -4 | 0 | | | 10 | 9.52 | -2.05 | 5.95 | 10 | 8.51 | 1.21 | 6.88 | 14 | 11.10 | 0.50 | 9.29 |
| 08_gt1r_20200228_0980_3 | | | | | | 94 | 8.91 | 2.63 | 6.20 | 93 | 7.24 | -2.38 | 5.49 | 93 | 10.46 | -7.16 | 8.06 |
| 08_gt1r_20200228_0980_3s | -2 | -0.2 | -0.6 | -2 | 0 | 94 | **8.70** | 1.93 | **6.06** | 93 | ***7.46*** | -3.06 | ***5.75*** | 93 | 10.44 | -7.15 | 8.06 |
| 08_gt1r_20200228_0980_3s0 | -2 | -0.2 | 0 | | | 94 | 8.85 | 2.53 | 6.19 | 93 | 7.23 | -2.46 | 5.55 | 93 | 10.44 | -7.15 | 8.06 |
| 08_gt2r_20200228_0980_3 | | | | | | 50 | 12.11 | -0.09 | 9.00 | 49 | 7.84 | 0.03 | 5.98 | 51 | 12.41 | -3.02 | 9.96 |
| 08_gt2r_20200228_0980_3s | 0 | 0 | -7.8 | 0 | 0 | 50 | ***14.45*** | -7.89 | ***11.24*** | 49 | ***11.04*** | -7.77 | ***9.43*** | 51 | 12.41 | -3.02 | 9.96 |
| 08_gt2r_20200228_0980_3s0 | 0 | 0 | 0 | | | 50 | 12.11 | -0.09 | 9.00 | 49 | 7.84 | 0.03 | 5.98 | 51 | 12.41 | -3.02 | 9.96 |

Numbers in bold highlight a marked improvement, numbers in italics a marked worsening. Across-track (xT) and Along-track (aT) corrections that seems contradictory for different beams have been marked with an asterisk (∗). The last characters on the file name (first column) denote the level of geolocation adjustment, files ending "_3" correspond to the ATL08 files as produced and reported, "_3s" to files that have been shifted in three dimensions, and "_3s0" to files that were only shifter horizontally ignoring the vertical correction.

## ACKNOWLEDGMENT

The authors are grateful to the investigators and sponsors that made the collection of the HDL in Mesoamerica possible; and which enabled this value-added research. NASA and NSIDC are also thanked for making the ICESat-2 data available, as is OpenAltimetry for allowing easy exploration of ATL08 data.

## REFERENCES

[1] *Thriving on Our Changing Planet: A Decadal Strategy for Earth Observation From Space*. Washington, DC, USA: National Academies Press, 2018, doi: 10.17226/24938.

[2] B. E. Schutz, H. J. Zwally, C. A. Shuman, D. Hancock, and J. P. DiMarzio, "Overview of the ICESat mission," *Geophys. Res. Lett.*, vol. 32, no. 21, Nov. 2005, doi: 10.1029/2005GL024009.

[3] T. Markus *et al.*, "The ice, cloud, and land elevation satellite-2 (ICESat-2): Science requirements, concept, and implementation," *Remote Sens. Environ.*, vol. 190, pp. 260–273, Mar. 2017, doi: 10.1016/j.rse.2016.12.029.

[4] Y. Pan, R. A. Birdsey, O. L. Phillips, and R. B. Jackson, "The structure, distribution, and biomass of the World's forests," *Annu. Rev. Ecol., Evol., Systematics*, vol. 44, no. 1, pp. 593–622, Nov. 2013, doi: 10.1146/annurev-ecolsys-110512-135914.

[5] Y. Malhi, D. D. Baldocchi, and P. G. Jarvis, "The carbon balance of tropical, temperate and boreal forests," *Plant Cell Environ.*, vol. 22, no. 6, pp. 715–740, 1999, doi: 10.1046/j.1365-3040.1999.00453.x.

[6] T. A. Gardner *et al.*, "Prospects for tropical forest biodiversity in a human-modified world," *Ecol. Lett.*, vol. 12, no. 6, pp. 561–582, Jun. 2009, doi: 10.1111/j.1461-0248.2009.01294.x.

[7] C. L. Glennie, W. E. Carter, R. L. Shrestha, and W. E. Dietrich, "Geodetic imaging with airborne Lidar: The Earth's surface revealed," *Rep. Prog. Phys.*, vol. 76, no. 8, Aug. 2013, Art. no. 086801, doi: 10.1088/0034-4885/76/8/086801.

[8] R. Dubayah *et al.*, "The global ecosystem dynamics investigation: High-resolution laser ranging of the Earth's forests and topography," *Sci. Remote Sens.*, vol. 1, Jun. 2020, Art. no. 100002, doi: 10.1016/j.srs.2020.100002.

[9] L. L. Narine, S. C. Popescu, and L. Malambo, "Using ICESat-2 to estimate and map forest aboveground biomass: A first example," *Remote Sens.*, vol. 12, no. 11, 2020, Art. no. 1824, doi: 10.3390/rs12111824.

[10] C. Wang *et al.*, "Ground elevation accuracy verification of ICESat-2 data: A case study in Alaska, USA," *Opt. Exp.*, vol. 27, no. 26, pp. 38168–38179, 2019.

[11] Y. Xing, J. Huang, A. Gruen, and L. Qin, "Assessing the performance of ICESat-2/ATLAS multi-channel photon data for estimating ground topography in forested Terrain," *Remote Sens.*, vol. 12, no. 13, 2020, Art. no. 1824, doi: 10.3390/rs12132084.

[12] X. Tian and J. Shan, "Comprehensive evaluation of the ICESat-2 ATL08 terrain product," *IEEE Trans. Geosci. Remote Sens.*, vol. 59, no. 10, pp. 8195–8209, Oct. 2021, doi: 10.1109/TGRS.2021.3051086.

[13] L. A. Neuenschwander and A. L. Magruder, "Canopy and terrain height retrievals with ICESat-2: A first look," *Remote Sens.*, vol. 11, no. 14, 2019, Art. no. 1721, doi: 10.3390/rs11141721.

[14] A. Neuenschwander, E. Guenther, J. C. White, L. Duncanson, and P. Montesano, "Validation of ICESat-2 terrain and canopy heights in boreal forests," *Remote Sens. Environ.*, vol. 251, Dec. 2020, Art. no. 112110, doi: 10.1016/j.rse.2020.112110.

[15] A. Liu, X. Cheng, and Z. Chen, "Performance evaluation of GEDI and ICESat-2 laser altimeter data for terrain and canopy height retrievals," *Remote Sens. Environ.*, vol. 264, Oct. 2021, Art. no. 112571, doi: 10.1016/j.rse.2021.112571.

[16] L. Malambo and S. C. Popescu, "Assessing the agreement of ICESat-2 terrain and canopy height with airborne lidar over US ecozones," *Remote Sens. Environ.*, vol. 266, Dec. 2021, Art. no. 112711, doi: 10.1016/j.rse.2021.112711.

[17] M. Queinnec, J. C. White, and N. C. Coops, "Comparing airborne and spaceborne photon-counting LiDAR canopy structural estimates across different boreal forest types," *Remote Sens. Environ.*, vol. 262, Sep. 2021, Art. no. 112510, doi: 10.1016/j.rse.2021.112510.

[18] A. Neuenschwander and K. Pitts, "Ice, cloud and land elevation satellite 2 (ICESat-2) algorithm theorethical basis document (ATBD) for land-vegetation along-track products (ATL08)," NASA, 2019.

[19] S. J. S. Khalsa *et al.*, "OpenAltimetry—Rapid analysis and visualization of spaceborne altimeter data," *Earth Sci. Informat.*, Sep. 2020, doi: 10.1007/s12145-020-00520-2.

[20] J. C. Fernandez-Diaz *et al.*, "Optimizing ground return detection through forest canopies with small footprint airborne mapping LiDAR," in *Proc. IEEE Geosci. Remote Sens. Symp.*, 2014, pp. 1963–1966.

[21] J. Fernandez-Diaz *et al.*, "Capability assessment and performance metrics for the titan multispectral mapping Lidar," *Remote Sens.*, vol. 8, no. 11, 2016, Art. no. 936.

[22] "ASPRS positional accuracy standards for digital geospatial data," *Photogramm. Eng. Remote Sens.*, vol. 81, no. 3, pp. A1–A26, Mar. 2015.

[23] C. T. Fisher *et al.*, "Identifying ancient settlement patterns through LiDAR in the mosquitia region of Honduras," *PLoS One*, vol. 11, no. 8, 2016, Art. no. e0159890, doi: 10.1371/journal.pone.0159890.

[24] M. A. Canuto *et al.*, "Ancient lowland Maya complexity as revealed by airborne laser scanning of northern Guatemala," *Science*, vol. 361, no. 6409, 2018, Art. no. eaau0137, doi: 10.1126/science.aau0137.

[25] T. W. Stanton *et al.*, "'Structure' density, area, and volume as complementary tools to understand Maya settlement: An analysis of lidar data along the great road between Coba and Yaxuna," *J. Archaeol. Sci., Rep.*, vol. 29, Feb. 2020, Art. no. 102178, doi: 10.1016/j.jasrep.2019.102178.

[26] W. M. Ringle, T. Gallareta Negrón, R. M. Ciau, K. E. Seligson, J. C. Fernandez-Diaz, and D. O. Zapata, "Lidar survey of ancient Maya settlement in the Puuc region of Yucatan, Mexico," *PLoS One*, vol. 16, no. 4, 2021, Art. no. e0249314, doi: 10.1371/journal.pone.0249314.

[27] T. Beach *et al.*, "The early anthropocene in tropical forests. Ancient Maya wetland fields revealed from laser scanning and multiproxy evidence," *Proc. Nat. Acad. Sci.*, vol. 116, pp. 21469–21477, 2019.

[28] I. Šprajc *et al.*, "Ancient Maya water management, agriculture, and society in the area of Chactún, Campeche, Mexico," *J. Anthropol. Archaeol.*, vol. 61, Mar. 2021, Art. no. 101261, doi: 10.1016/j.jaa.2020.101261.

[29] C. Golden *et al.*, "Airborne lidar survey, density-based clustering, and ancient maya settlement in the upper usumacinta river region of Mexico and Guatemala," *Remote Sens.*, vol. 13, no. 20, 2021, Art. no. 4109, doi: 10.3390/rs13204109.

[30] C. Jin, C. Oh, S. Shin, N. Wilfred Njungwi, and C. Choi, "A comparative study to evaluate accuracy on canopy height and density using UAV, ALS, and fieldwork," *Forests*, vol. 11, no. 2, 2020, Art. no. 241, doi: 10.3390/f11020241.

[31] *LAS Specification Version 1.2*. Bethesda, MD, USA: American Society for Photogrammetry and Remote Sensing, 2005.

[32] *LAS Specification Version 1.4—R14*. Bethesda, Maryland: American Society for Photogrammetry and Remote Sensing, Nov. 2011. [Online]. Available: http://www.asprs.org/wp-content/uploads/2019/03/LAS_1_4_r14.pdf

[33] J. Fernandez-Diaz, W. Carter, R. Shrestha, and C. Glennie, "Now you see it … now you don't: Understanding airborne mapping LiDAR collection and data product generation for archaeological research in Mesoamerica," *Remote Sens.*, vol. 6, no. 10, pp. 9951–10001, 2014.

[34] L. A. Magruder, K. M. Brunt, and M. Alonzo, "Early ICESat-2 on-orbit geolocation validation using ground-based corner cube retro-reflectors," *Remote Sens.*, vol. 12, no. 21, 2020, Art. no. 3653, doi: 10.3390/rs12213653.

[35] L. Magruder, K. Brunt, T. Neumann, B. Klotz, and M. Alonzo, "Passive ground-based optical techniques for monitoring the on-orbit ICESat-2 altimeter geolocation and footprint diameter," *Earth Space Sci.*, vol. 8, no. 10, Oct. 2021, Art. no. e2020EA001414, doi: 10.1029/2020EA001414.

[36] I. Fayad *et al.*, "Canopy height estimation in French Guiana with LiDAR ICESat/GLAS data using principal component analysis and random forest regressions," *Remote Sens.*, vol. 6, no. 12, pp. 11883–11914, 2014, doi: 10.3390/rs61211883.

[37] N. Baghdadi *et al.*, "Testing different methods of forest height and aboveground biomass estimations from ICESat/GLAS data in eucalyptus plantations in Brazil," *IEEE J. Sel. Topics Appl. Earth Observ. Remote Sens.*, vol. 7, no. 1, pp. 290–299, Jan. 2014, doi: 10.1109/JSTARS.2013.2261978.

[38] "GLAS/ICESat L1 and L2 global altimetry data, version 33, 34, user guide," National snow and ice data center. [Online]. Available: https://nsidc.org/sites/nsidc.org/files/MULTI-GLA01-V033-V034-UserGuide.pdf

[39] S. C. Popescu, K. Zhao, A. Neuenschwander, and C. Lin, "Satellite lidar vs. small footprint airborne lidar: Comparing the accuracy of aboveground biomass estimates and forest structure metrics at footprint level," *Remote Sens. Environ.*, vol. 115, no. 11, pp. 2786–2797, Nov. 2011, doi: 10.1016/j.rse.2011.01.026.

[40] F. Enßle, J. Heinzel, and B. Koch, "Accuracy of vegetation height and terrain elevation derived from ICESat/GLAS in forested areas," *Int. J. Appl. Earth Observ. Geoinf.*, vol. 31, pp. 37–44, Sep. 2014, doi: 10.1016/j.jag.2014.02.009.

[41] M. Hayashi, N. Saigusa, H. Oguma, and Y. Yamagata, "Forest canopy height estimation using ICESat/GLAS data and error factor analysis in Hokkaido, Japan," *ISPRS J. Photogramm. Remote Sens.*, vol. 81, pp. 12–18, Jul. 2013, doi: 10.1016/j.isprsjprs.2013.04.004.

[42] M. A. Lefsky, "A global forest canopy height map from the moderate resolution imaging spectroradiometer and the geoscience laser altimeter system," *Geophys. Res. Lett.*, vol. 37, Aug. 2010, Art. no. 15, doi: 10.1029/2010GL043622.

[43] C. E. Doughty, M. L. Goulden, S. D. Miller, and H. R. da Rocha, "Circadian rhythms constrain leaf and canopy gas exchange in an Amazonian forest," *Geophys. Res. Lett.*, vol. 33, no. 15, Aug. 2006, Art. no. L15404, doi: 10.1029/2006GL026750.

[44] Y. Malhi, "The productivity, metabolism and carbon cycle of tropical forest vegetation," *J. Ecol.*, vol. 100, no. 1, pp. 65–75, Jan. 2012, doi: 10.1111/j.1365-2745.2011.01916.x.

[45] J. Xiao, J. B. Fisher, H. Hashimoto, K. Ichii, and N. C. Parazoo, "Emerging satellite observations for diurnal cycling of ecosystem processes," *Nature Plants*, vol. 7, no. 7, pp. 877–887, Jul. 2021, doi: 10.1038/s41477-021-00952-8.

[46] P. Potapov *et al.*, "Mapping global forest canopy height through integration of GEDI and landsat data," *Remote Sens. Environ.*, vol. 253, Feb. 2021, Art. no. 112165, doi: 10.1016/j.rse.2020.112165.

[47] S. P. Healey *et al.*, "CMS: GLAS lidar-derived global estimates of forest canopy height, 2004–2008," 2015, doi: 10.3334/ORNLDAAC/1271. [Online]. Available: https://daac.ornl.gov/CMS/guides/LIDAR_FOREST_CANOPY_HEIGHTS.html

**Juan Carlos Fernandez-Diaz** (Member, IEEE) received the B.Sc. degree in electrical and industrial engineering from Universidad Nacional Autonoma de Honduras, Tegucigalpa, Honduras, in 2001, and the M.Sc. and Ph.D. degrees in geosensing systems engineering from the University of Florida, Gainesville, FL, USA, in 2007 and 2010, respectively.

He is currently a Research Assistant Professor with the University of Houston, Houston, TX, USA, and Co-PI of the NSF supported National Center for Airborne Laser Mapping. His research interest includes 3-D characterization with active remote sensing.

**Mariya Velikova** received the bachelor's degree in applied geophysics from the University of Mining and Geology, Sofia, Bulgaria, in 2011 and the joint master's degree in space science and technology from the Lule University of Technology, Luleå, Sweden, and Paul Sabatier University, Toulouse, France, in 2018. She is currently working toward the Ph.D. degree in geosensing systems and engineering with the University of Houston, Houston, TX, USA.

Her research interests include lidar mapping and deep learning applied on lidar point clouds.

**Craig L. Glennie** (Member, IEEE) received the B.Sc. and Ph.D. degrees in geomatics engineering from the University of Calgary, Calgary, AB, Canada, in 1996 and 1999, respectively.

He is currently a Professor of Civil and Environmental Engineering with the University of Houston, Houston, TX, USA, where he is also the Principal Investigator and Director of the NSF supported National Center for Airborne Laser Mapping Facility. His research interests include the design, development, and operation of kinematic geodesy and remote sensing systems.